Continental Shelf Research 146 (2017) 58–81

Contents lists available at ScienceDirect

Continental Shelf Research

journal homepage: www.elsevier.com/locate/csr

Research papers

Modeling salt intrusion in the San Francisco Estuary prior to anthropogenic influence

S.W. Andrews[a,*], E.S. Gross[a,b], P.H. Hutton[c]

[a] Resource Management Associates, 1756 Picasso Avenue, Suite G, Davis, CA 95618, USA
[b] Center for Watershed Sciences, University of California Davis, One Shields Avenue, Davis, CA 95616, USA
[c] Metropolitan Water District of Southern California, 1121 L Street, Suite 900, Sacramento, CA 95814, USA

ARTICLE INFO

Keywords:
San Francisco Estuary
Sacramento–San Joaquin Delta
Salt intrusion
Hydrodynamic model
Tidal hydrodynamics
Hydrologic change

ABSTRACT

Anthropogenic changes have dramatically transformed the upper San Francisco Estuary over the past two centuries. Key changes influencing the region's hydrology and hydrodynamics include land use changes, levee construction and channel modifications, upstream reservoir construction, and out-of-basin water exports. In order to examine how these changes have altered the physical characteristics of the estuary, 3-D hydrodynamic models were constructed to study the system in its "pre-development" condition, prior to significant modern anthropogenic influence, and in its contemporary condition. The pre-development system model was calibrated by varying marsh plain elevations in order to match sparse observations of tidal characteristics; the contemporary system model was calibrated to observed flow, stage, and salinity data. A recent three-year period covering a wide range of flow conditions was used to compare and contrast the hydrodynamic behavior of the two systems. While the contemporary model simulation assumed historical observed boundary conditions, the pre-development model simulation assumed conditions thought to exist prior to the alterations of the past two centuries. The relationship between estuary outflow and the longitudinal distance from the estuary mouth to the 2 psu bottom salinity isohaline (X2) was analyzed. Salt intrusion in the pre-development system was found to be slightly more sensitive to outflow and responded faster to changes in outflow than in the contemporary system. Changes in estuary outflows were responsible for more of the salt intrusion differences between the two systems than were changes in estuary geometry and bathymetry. An analysis of the physical mechanisms contributing to salt intrusion found tidal trapping and other unsteady processes to be more important in the pre-development estuary than in the contemporary one. In both systems, steady processes such as estuarine circulation were strongest during neap tides and unsteady salt intrusion processes were strongest during spring tides, resulting in limited spring-neap variability in salt intrusion.

1. Introduction

Over the past two centuries, the San Francisco Estuary and its watershed have been significantly modified by human development. These changes have altered both the hydrology and geometry of the estuary. Ninety eight percent of the emergent tidal wetlands of the upper estuary have been disconnected from adjacent channels with levees, drained, and converted to agriculture (Atwater et al., 1979). Oxidation and erosion of these organic soils has caused land subsidence, and where levee failure has occurred, the creation of large areas of novel subtidal habitat within the estuary (Mount and Twiss, 2005). Main channels throughout the estuary were widened, deepened, and connected with cross channels to improve navigation. A myriad of blind tidal sloughs were removed (Whipple et al., 2012). The geomorphology of the estuary has changed in response to modifications in upstream sediment supply (Barnard et al., 2013) and sea level rise (NOAA, 2016). Estuary inflow has changed in magnitude and timing due to reservoir construction and land use changes in the upper watershed (Fox et al., 1990). Water use within the estuary has been affected by wetland removal, local diversions and return flows, and out of basin diversions (Lund et al., 2007). A network of gates, temporary flow barriers, and other hydraulic structures was installed, allowing managers some control over the distribution of flows through the upper estuary.

These anthropogenic changes will necessarily have effects on salt intrusion, which is dependent on 1) net advection driven by freshwater outflows, and 2) a host of geometry and bathymetry dependent salt intrusion mechanisms (Fischer et al., 1979). The seasonal timing of freshwater outflows to the San Francisco Bay has been influenced by

* Corresponding author.
E-mail address: steve@rmanet.com (S.W. Andrews).

http://dx.doi.org/10.1016/j.csr.2017.07.010
Received 1 August 2016; Received in revised form 2 May 2017; Accepted 20 July 2017
Available online 25 July 2017

water management policies in California, which are generally characterized by reservoir impoundment in the winter and spring and reservoir release in the summer. This has decreased seasonal variability in salt intrusion and had a stabilizing effect on salinity (Hutton et al., 2015). Recent studies suggest that increases in urban and agricultural water use from the pre development period have been balanced by decreases in evapotranspiration by native vegetation, leading to little long term change in average annual estuary outflow (Fox et al., 2015; CDWR, 2016f). This would suggest a correspondingly small long term change in average annual salinity intrusion.

The effect of long term changes in the geometry and bathymetry of the estuary is dependent upon the physical mechanisms which result in salt intrusion in an estuary. The best known is gravitational circulation, in which dense water intrudes landward into the estuary near the bed and estuarine water flows seaward near the surface (Geyer and MacCready, 2014). Strain Induced Periodic Stratification (SIPS) results from an asymmetric shear in tidal currents between flood and ebb and causes a similar estuarine circulation pattern (Simpson et al., 1990). Additional physical mechanisms contributing to estuarine circulation have been identified (Lerczak and Geyer, 2004). Salt intrusion can also occur due to tidal dispersion mechanisms such as tidal pumping (Stommel and Farmer, 1953) and tidal trapping (Fischer et al., 1979). In the San Francisco Estuary, tidal pumping is known to be an important salt transport mechanism near the Golden Gate (Fram et al., 2007). Estuarine circulation is important for salt transport in the saline portion of the northern estuary (Stacey et al., 2001), and tidal trapping mechanisms are also known to be important (MacVean and Stacey, 2011). Because the strength of these salt intrusion mechanisms varies with water column depth (e.g., Ralston et al., 2008) changes in the bathymetry of the estuary and mean sea level are expected to influence salt intrusion.

Changes in the salinity distribution in an estuary impact estuarine ecology (Kimmerer, 2002). For example, most estuarine species are associated with a limited range of salinity. In the San Francisco Estuary, the observed abundance of several pelagic organisms has been correlated with salt intrusion length (Jassby et al., 1995; Kimmerer et al., 2009, 2013). The intrusion length metric used by Jassby et al. (1995) and subsequent research in the area is X2, defined as the distance from the inlet at the Golden Gate to the location of the tidally averaged 2 psu near bed salinity. An observed decrease in the abundance of these organisms has resulted in the regulation of X2 during specified periods of ecological importance (CSWRCB, 1999). The geographical location of ecologically important areas such as estuarine turbidity maxima, entrapment zones, and low salinity zones are also controlled by salt intrusion mechanisms (Schoellhamer, 2001; Kimmerer et al., 2013). As a result of the geometry of the San Francisco Estuary, small changes in salt intrusion may result in large changes in the aerial extent of these areas (Kimmerer et al., 2013).

The net effect of anthropogenic changes to hydrology and geometry on the salinity distribution in the San Francisco Estuary is unknown. Historical observations of salinity intrusion in the early 1900s indicate a more seasonably variable salt intrusion regime than today (Hyatt, 1931). These observations were made prior to the construction of major reservoirs in the watershed but after the reclamation of the majority of tidal wetland in the upper estuary. Some ecologists believe that a more variable salinity regime would benefit aquatic species native to the estuary by limiting the extent of non native species (e.g., Moyle et al., 2010). However, due to a lack of quantitative salinity observations, the actual salinity regime prior to anthropogenic influence remains unknown. Even the presence of stronger variability remains an untested hypothesis.

The main objective of this study is to quantify salt intrusion in the San Francisco Estuary under its pre development condition (circa 1850) and in its contemporary condition. Because the strength of salt transport mechanisms depends strongly on bathymetry, the best way to estimate the effects of alterations in estuarine geometry on salinity is by using a mechanistic 3 D hydrodynamic model. In this paper we describe the construction and calibration of hydrodynamic models to reflect conditions in both the pre development and contemporary estuary. Our work assumed pre development inflow hydrology that was estimated by the California Department of Water Resources (CDWR) (CDWR, 2016f) based on land and water use conditions thought to exist prior to 1850 (Fox et al., 2015; Howes et al., 2015). Using time series of the salt intrusion metric X2 predicted by the models, the relationship of X2 with estuarine outflow is compared. This type of analysis addresses both the sensitivity of X2 to steady outflow and the time scale of change in X2 to changes in outflow. Additionally, it allows us to distinguish changes in modeled X2 resulting from altered inflow hydrology from those resulting from altered estuarine geometry and bathymetry. Since sea level rise is effectively a change in relative bathymetry, the effect of its changes on X2 are assessed in conjunction with other estuary geometry and bathymetry modifications.

We then estimate the relative contribution of different physical mechanisms on salt fluxes into the upper estuary using an isohaline coordinate approach (MacCready, 2011). Fluxes due to estuarine circulation processes and unsteady tidal processes are quantified for both the contemporary and pre development estuary throughout the simulation period. This analysis provides insight to the effect of large scale landscape changes not only on salt intrusion length but also on the physical mechanisms contributing to salt intrusion.

Understanding salinity intrusion in the pre development San Francisco Estuary should help guide future restoration efforts and management and may offer insight into the adaptations of native aquatic species in this sensitive region. Many of the changes that have taken place in the San Francisco Estuary over the last two centuries land reclamation, altered hydrology, channel modifications for navigation, sea level rise are common to other estuaries (see for example, Wang et al., 2015). Lessons learned from this study can increase understanding and support restoration efforts in these systems as well.

2. Site description

The San Francisco Estuary is the largest estuary on the Pacific Coast of the United States, with a watershed covering 40% of the area of the California, and is composed of a series of interconnected embayments, rivers, sloughs, and marshes (Kimmerer, 2004; Conomos, 1979). The focus of this study is the upper portion of the estuary, including Carquinez Strait, Suisun Bay, Suisun Marsh, and the Sacramento San Joaquin Delta (hereafter referred to as “the Delta”) (Fig. 1). Regional topography confines the estuary to relatively narrow outlets at Carquinez Strait and near the confluence of the Sacramento and San Joaquin Rivers. Bathymetry through Suisun Bay is complex and characterized by channels typically ranging from 10 m to 20 m deep and extensive shoal and intertidal regions.

The bathymetry and channel connectivity of the Delta and Suisun Marsh have changed substantially between 1850 and today. In the pre development condition, the Delta and Suisun Marsh were characterized by relatively shallow and sinuous channels, numerous blind sloughs and extensive intertidal marsh plain (Whipple et al., 2012; Manfree, 2014). The northern region of the Delta was dominated by wide flood basins inundated in winter and spring. The central region of the Delta was dominated by tidal influence, and the southern Delta consisted of numerous distributary rivers. These areas have since undergone extensive modifications to dike and isolate productive intertidal land for agriculture and straighten, widen, deepen, and connect main channels for navigation. Levees were breached in some locations, leading to the creation of large shallow subtidal areas.

The San Francisco Estuary has mixed diurnal and semidiurnal tides. Spring neap variation is strong, and spring tide amplitudes can be as high as double neap tide amplitudes (Cheng et al., 1993). The region’s climate is Mediterranean, characterized by wet winters and dry summers. Freshwater inflow to the estuary is highly variable, with most

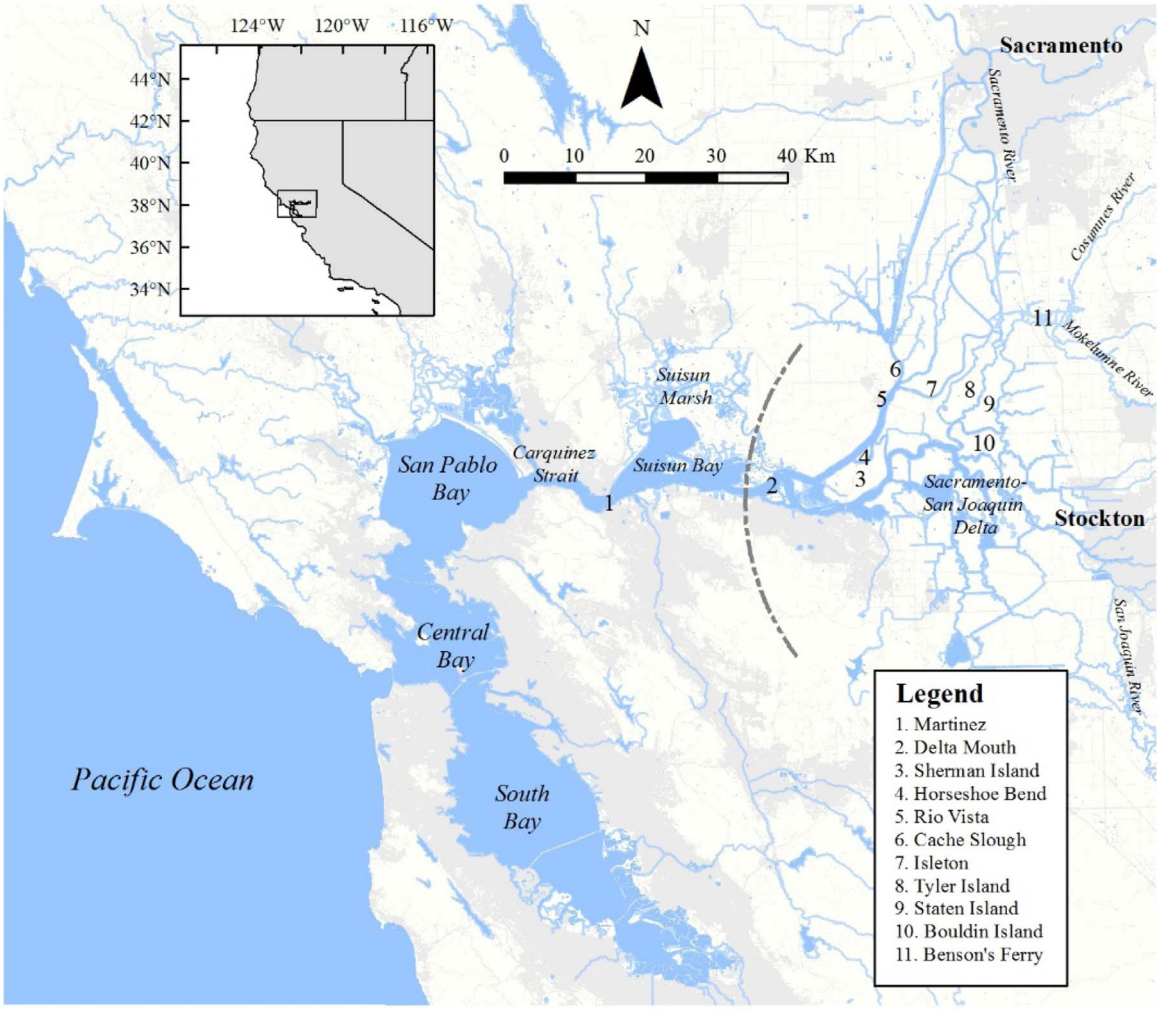

Fig. 1. San Francisco Estuary study area. Regions and sites labeled in the figure are referred to in the text.

inflow originating from the Sacramento River and, to a lesser extent, the San Joaquin River. Winter and spring inflows typically rise following periods of storms and snowmelt. In the pre development system, low net estuary outflow conditions occurred in the late summer and early fall as a result of low inflows and water use by extensive emergent vegetation (CDWR, 2016f). Contemporary flow conditions during this period are highly influenced by state and federal water management projects that release stored water to meet multiple objectives. Salt intrusion and stratification vary seasonally with freshwater inflow, typically resulting in partially mixed conditions in the seaward portion of the estuary and well mixed conditions within the Delta.

3. Methods

This section briefly describes the model construction and calibration process, simulations, and analysis methods related to salt intrusion length and flux. Using the same 3 D hydrodynamic engine, two models were constructed to study the San Francisco Estuary in its pre development condition and in its contemporary condition. A unique model of the contemporary system was created to provide 1) confidence in the modeling framework by demonstrating accurate simulation of the contemporary system, where much observed data is available for model evaluation, and 2) a comparison to the pre development system model with all model parameters other than inflow hydrology, sea level, and grid geometry and bathymetry held constant.

3.1. Hydrodynamic models

The UnTRIM model (Casulli and Walters, 2000; Casulli and Zanolli, 2005; Casulli and Stelling, 2010) was chosen as the hydrodynamic engine for this study. UnTRIM numerically solves the 3 D Reynolds averaged Navier Stokes equations for conservation of fluid volume and momentum on an unstructured grid. Model outputs are predicted water velocities, water surface elevations, and salinity. UnTRIM accounts for the relevant physical processes related to salt intrusion, is well suited to wetting and drying simulations (Casulli, 2009), and allows for subgrid scale representation of bathymetry. Vertical turbulent mixing in the model was estimated using the k ε version of a Generic Length Scale (GLS) closure with parameter values from Warner et al. (2005). Bed friction was parameterized using a quadratic stress formula and specified bed roughness height, z_0.

Model grid bathymetry and boundary condition locations for the contemporary San Francisco Estuary are shown in Fig. 2. Typical cell spacing was 150 m, and 1 m layer spacing was used in the vertical. Bathymetry was set using a digital elevation model (DEM) of the San Francisco Estuary developed using a large number of bathymetric surveys (Wang and Ateljevich, 2012). Major river and diversion boundary conditions were prescribed using data obtained from United States Geological Survey (USGS) monitoring sites and provided by CDWR (2016d). Local agricultural diversions, return flows, evaporation, precipitation, and groundwater seepage (collectively referred to as net channel depletions) were prescribed at 258 locations throughout the Delta using estimates from CDWR (2016e); outside of the Delta,

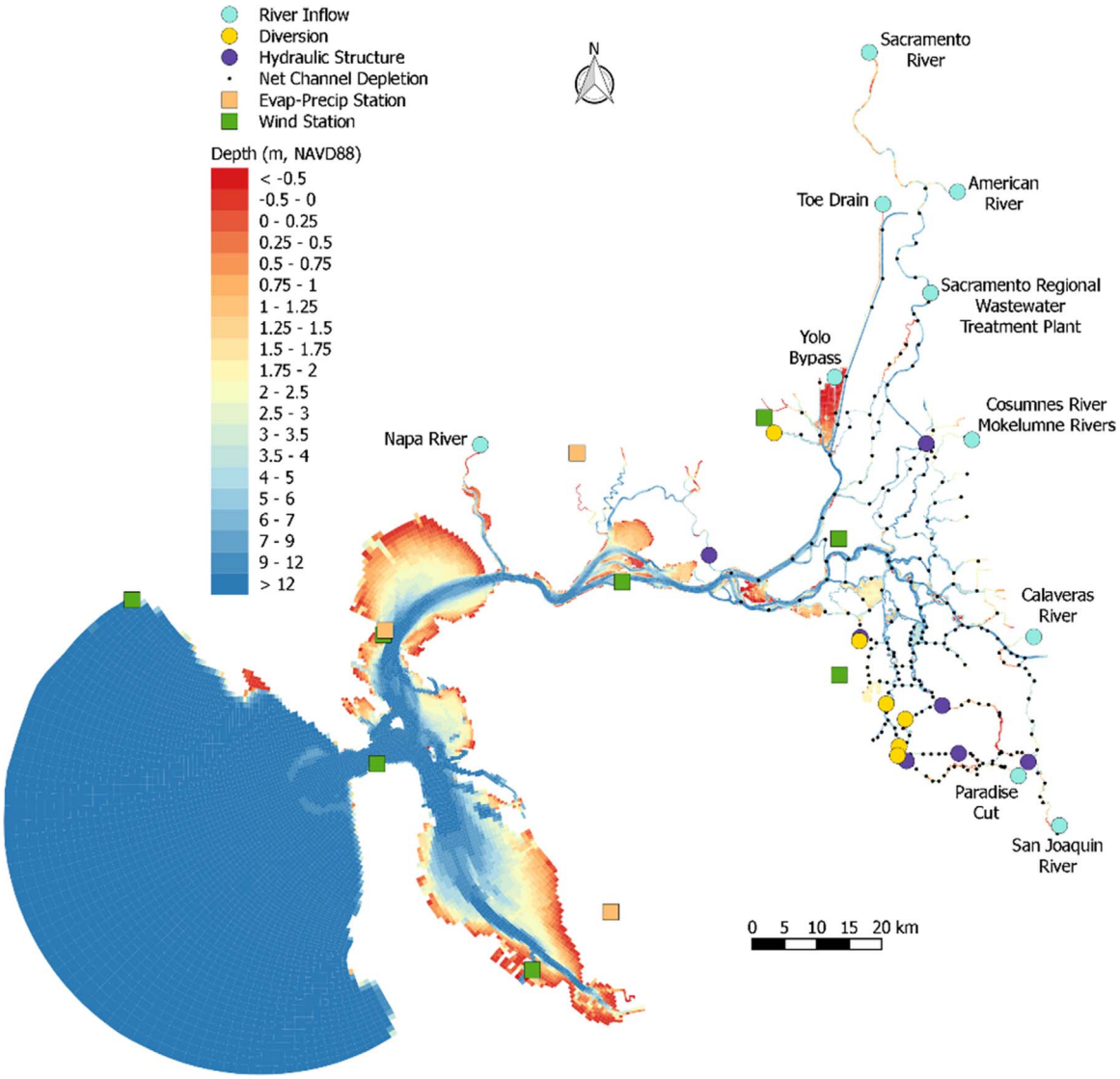

Fig. 2. Contemporary San Francisco Estuary model grid and bathymetry. Model boundary condition locations are shown for river inflows, diversions, net channel depletions, and hydraulic structures. Station locations used in setting regional wind and evaporation-precipitation model inputs are also shown.

measured evaporation and precipitation rates were used (CDWR, 2016b). Observed water levels at Point Reyes were used as the offshore boundary condition, and offshore salinity was set to a constant 33.5 psu.

Model output was compared against observed flow, stage, and salinity data collected at continuous monitoring stations throughout the estuary (CDWR, 2016a). The predicted vertical salinity structure was also compared against monthly observations collected by the USGS on a longitudinal transect from the Golden Gate inlet upstream to Rio Vista (USGS, 2016).

A separate unstructured orthogonal grid was developed for the pre development model simulations (Fig. 3). In the upper estuary, the grid was developed based on channel planform geometry derived from a large number of historical maps, imagery, and other sources as reported by Whipple et al. (2012) and Manfree (2014). The lateral extents of the grid were chosen to correspond to the extreme upper limit of seasonal inundation. Seaward of Carquinez Strait, the grid and bathymetry were identical to the contemporary estuary model. Bathymetry was set using a DEM developed by interpolating historical sounding data, thalweg depth measurements, and natural levee elevations along major channels to create a continuous, smooth DEM (SFEI ASC, 2014). Marsh plain elevations were specified so that model simulations provided tidal range and inundation frequency predictions consistent with historical observations.

Boundary inflows for the pre development model were extracted from hydrologic simulations reported by CDWR (2016f). In these si mulations, historical runoff was routed through unimpaired upper watersheds and the Central Valley as they were thought to exist prior to anthropogenic modifications of the past 160 years. Descriptions of methods and model assumptions relating to pre development land use and evapotranspiration are given in Fox et al. (2015) and Howes et al. (2015). Observed water levels at Point Reyes were shifted −0.31 m to account for sea level rise based on an average trend of 1.92 mm per year (NOAA, 2016).

Historical observed data for comparison with pre development model output were reported in Whipple et al. (2012) and are given in Appendix A. Observations were of three types: tidal range in channels, marsh plain inundation frequency, and depth of marsh plain inunda tion. For observations of marsh plain inundation depth, the tide at the time of the observation (spring or neap) was specified in some in stances. Data extracted from the historical accounts are generally un certain as the exact location of the measurement, and observations are typically rough estimates. In addition to specific historical observations, information about marsh plain inundation flow patterns and the spatial

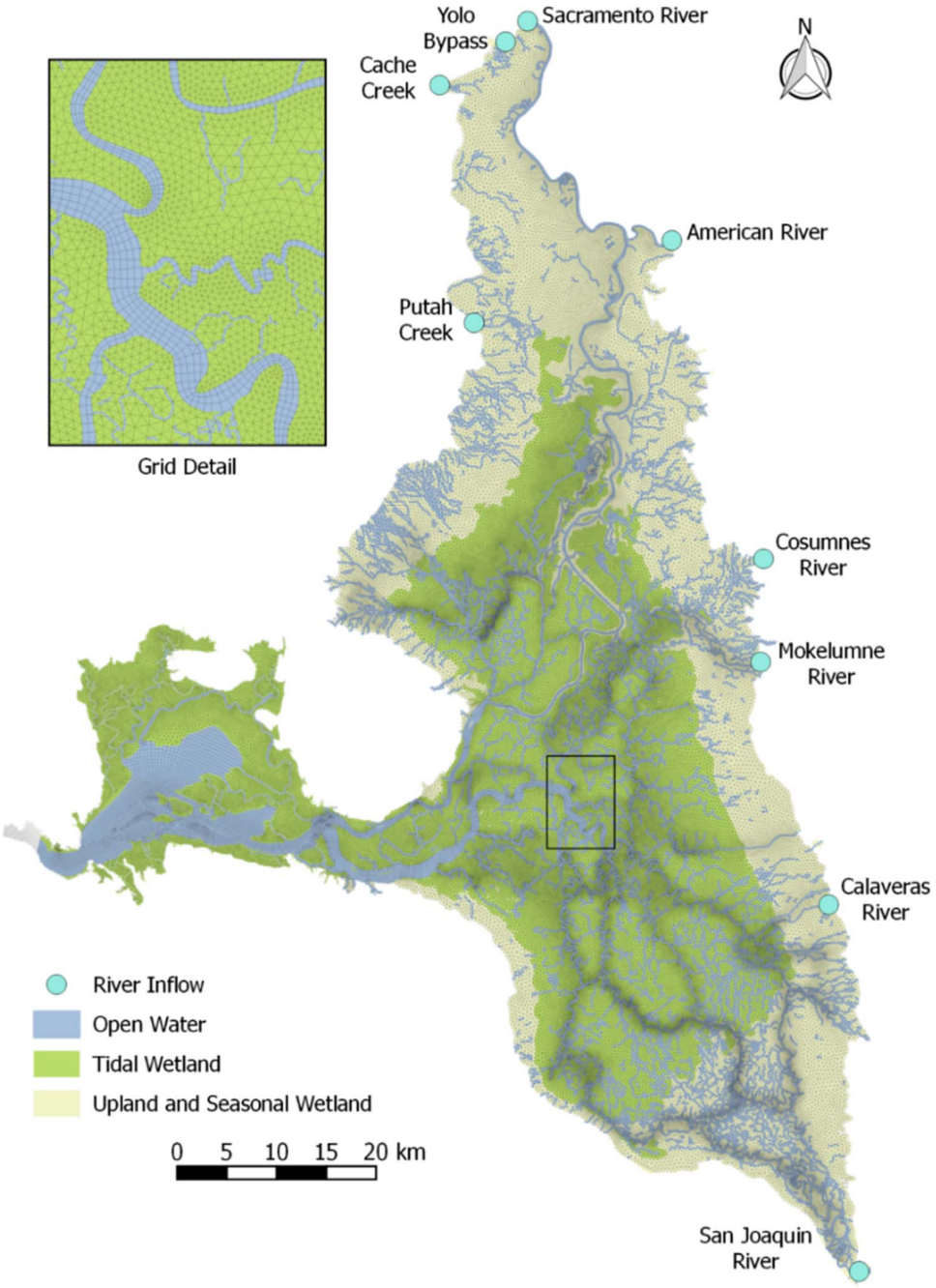

Fig. 3. Pre-development San Francisco Estuary model grid (landward of Carquinez Strait) and habitat type. Habitat was classified and delimited by Whipple et al. (2012) and Manfree (2014). The grid seaward of Carquinez Strait is identical to the contemporary San Francisco Estuary model grid. Boundary conditions locations are shown for river inflows.

extent of freshwater tidal habitat was used for calibration (Whipple et al., 2012).

3.2. Model simulations

The model simulation period was chosen as February 2006 through October 2008 in order to span wet, dry, and critically dry water years (CDWR, 2016c). Time series of net daily estuary inflows minus water losses for diversions and evapotranspiration are shown in Fig. 4. Net flows ranged from over 7000 $m^3 s^{-1}$ in April 2006 to below 50 $m^3 s^{-1}$ for the pre development system during summer and fall 2007 and 2008. In 2007 and 2008, contemporary flows were generally lower than pre development flows in the spring and early summer and higher in the late summer and early fall.

In order to compare pre development model predictions against historical observations, spatial maps of tidal characteristics were calculated. Tidal characteristics were calculated as monthly averages because 1) the exact date or time of the year of individual observations was generally unspecified and 2) tidal characteristics vary seasonally. Reported values for comparison with observations are given as the minimum, median, and maximum of the monthly values. Tidal range was calculated as the difference between mean higher high water and mean lower low water (great diurnal range), as the historical reports are generally believed to correspond to this metric. Tidal inundation frequency was determined as the number of wetting drying cycles ex perienced by each computational cell, using a minimum depth threshold of 2 cm to declare a cell wet.

3.3. Intrusion length analysis

Two important metrics of salt intrusion are intrusion length (X2) and the time scale of adjustment of this length to changes in estuary

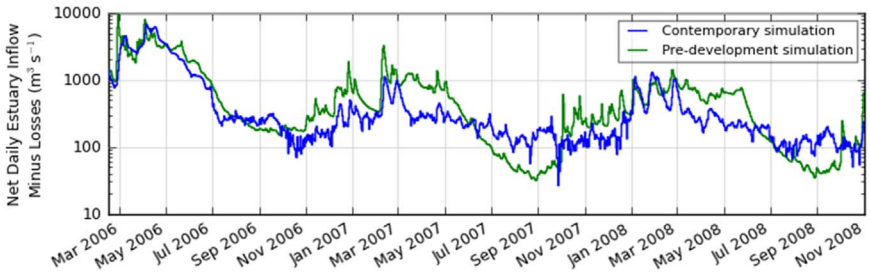

Fig. 4. Comparison of contemporary and pre-development simulation net estuary inflows minus water losses for diversions and evapotranspiration.

outflow. These topics have been studied in the San Francisco Estuary and other settings by analysis of field observations and empirical fitting (Jassby et al., 1995; Monismith et al., 2002; Hutton et al., 2015; Monismith, 2017), by semi analytical approaches with empirical parameters (Monismith et al., 2002; MacCready, 2007; Ralston et al., 2008; Lerczak et al., 2009; Monismith, 2017), and through the use of hydrodynamic models (Gross et al., 2009; MacWilliams et al., 2015).

In Jassby et al. (1995), the daily position of observed X2 was esti mated by interpolation between fixed salinity stations and a time series regression relation involving the previous day's X2 and the current day's outflow, Q

$$X2(t) = \theta_0 + \alpha\, X2(t-1) + \gamma_J \log Q(t) \tag{1}$$

where θ_0, α and γ_J are fitting parameters. In this approach, the time scale for adjustment to changes in flow is $\tau_J = 1/(1-\alpha)$.

Monismith et al. (2002) provided a revised regression analysis that retained the influence of the previous day's X2, but with a flow de pendence term derived by a simplified analysis of relevant physics, following Hansen and Rattray (1965)

$$X2(t) = \alpha\, X2(t-1) + (1-\alpha)\,\beta\, Q(t)^{\gamma} \tag{2}$$

where θ_0 and$\gamma$are fitting parameters. Since α is the weight of the pre vious day's X2 in both equations, they have the same time scale of adjustment (τ_J). In MacWilliams et al. (2015), the weight was allowed to vary linearly with flow to allow faster response of salt intrusion length at high flow

$$X2(t) = \alpha(t)\, X2(t-1) + (1-\alpha(t))\,\beta\, Q(t)^{\gamma} \tag{3}$$

$$\alpha(t) = \min[1,\max[0,mQ(t)+b]] \tag{4}$$

where α is bounded between zero and one, and m and b are fitting parameters. A significant improvement in accuracy of the time series regression was achieved with this modification (MacWilliams et al., 2015). Hutton et al. (2015) estimated daily X2 using the steady form of Eq. (2)

$$X2(t) = \beta Q_{ant}(t)^{\gamma} \tag{5}$$

where Q_{ant} is antecedent outflow and incorporates a time history of the outflow as follows (Denton, 1993)

$$\frac{dQ_{ant}(t)}{dt} = \frac{(Q(t) - Q_{ant}(t))Q_{ant}(t)}{\beta_G} \tag{6}$$

In Eq. (6), β_G is a fitting parameter ($m^3\ s^{-1}$ days) and the time scale for the adjustment of X2 to changes in flow is

$$\tau = \beta_G / Q_{ant} \tag{7}$$

In this analysis, X2 was calculated from daily averaged bottom salinity for each simulation; values were estimated by linear inter polation of data reported at 1 km intervals along the transects shown in Fig. 5. When X2 was located landward of the Sacramento San Joaquin confluence, the average of X2 along the Sacramento and San Joaquin River transects was used. Because of differences in channel configura tion, the pre development and contemporary system transects diverge in certain locations; to facilitate comparison between the two systems, pre development transect distances were mapped to contemporary distances so that X2 at the same geographical location in both systems had the same value.

A relationship between estuary outflow and X2 was developed fol lowing the approach of Hutton et al. (2015). This approach was selected because, unlike other approaches, it is mathematically defined for ne gative outflow values. This feature was important for the analysis, as negative outflow events are common in the pre development simulation and are associated with low inflows in phase with spring tide filling of the estuary. The free parameters in Eq. (5) and Eq. (6) (β, γ, and β_G) were simultaneously fit to the hydrodynamic model predicted X2 using the Levenberg Marquardt nonlinear least squares fitting method (Levenberg, 1944). Tidally averaged flow at Martinez predicted by the model was used to represent net Delta outflow, $Q(t)$, in Eq. (6).

3.4. Salt flux analysis

The X2 regression analysis conveniently represents differences in the extent of salt intrusion between the two systems using three para meters. However, information about the physical mechanisms re sponsible for the differences can be derived by analyzing the model predicted salt fluxes into the upper estuary. Following MacCready (2011), Chen et al. (2012), and Rayson et al. (In preparation), fluxes are examined using isohaline coordinates. We apply this analysis to esti mate salt influx from two categories: steady processes such as estuarine circulation, and unsteady processes such as tidal trapping.

The isohaline approach to calculating flows and salt fluxes through a cross section was described by MacCready (2011), who defined tid ally averaged flow with salinity greater than s as

$$Q(s) \equiv \left\langle \int_{A_s} u\, dA \right\rangle \tag{8}$$

where A_s is the cross sectional area having salinity greater than s and angle brackets denote a tidal average. The flow for a particular salinity class is given by the derivative of Eq. (8), although in practice model results are binned by salinity class. The portion of the flow bringing water landward into the estuary (Q_{in}) is defined as the integral of Q over the inflowing portion of the cross section. The outflowing component (Q_{out}) is defined analogously,

$$Q_{in} \equiv \int \frac{-\partial Q}{\partial s}\bigg|_{n} ds, \qquad Q_{out} \equiv \int \frac{-\partial Q}{\partial s}\bigg|_{out} ds \tag{9}$$

and $Q_{in} + Q_{out} = -Q_{riv}$, the net river outflow. In order to be consistent with MacCready (2011) and other estuarine researchers, this analysis uses the convention that landward flow and fluxes into the estuary are positive. In contrast, positive river flow (Q_{riv}) indicates net outflow. Salt fluxes and flux weighted salinities are defined as

$$F_{in} \equiv \int s \frac{-\partial Q}{\partial s}\bigg|_{in} ds, \qquad F_{out} \equiv \int s \frac{-\partial Q}{\partial s}\bigg|_{out} ds$$
$$s_{in} \equiv \frac{F_{in}}{Q_{in}}, \qquad s_{out} \equiv \frac{F_{out}}{Q_{out}} \tag{10}$$

This method of analysis captures flows and salt flux from both steady subtidal processes and unsteady tidal processes, and is thus re ferred to as a "total exchange flow" analysis. The net flux of salt into the

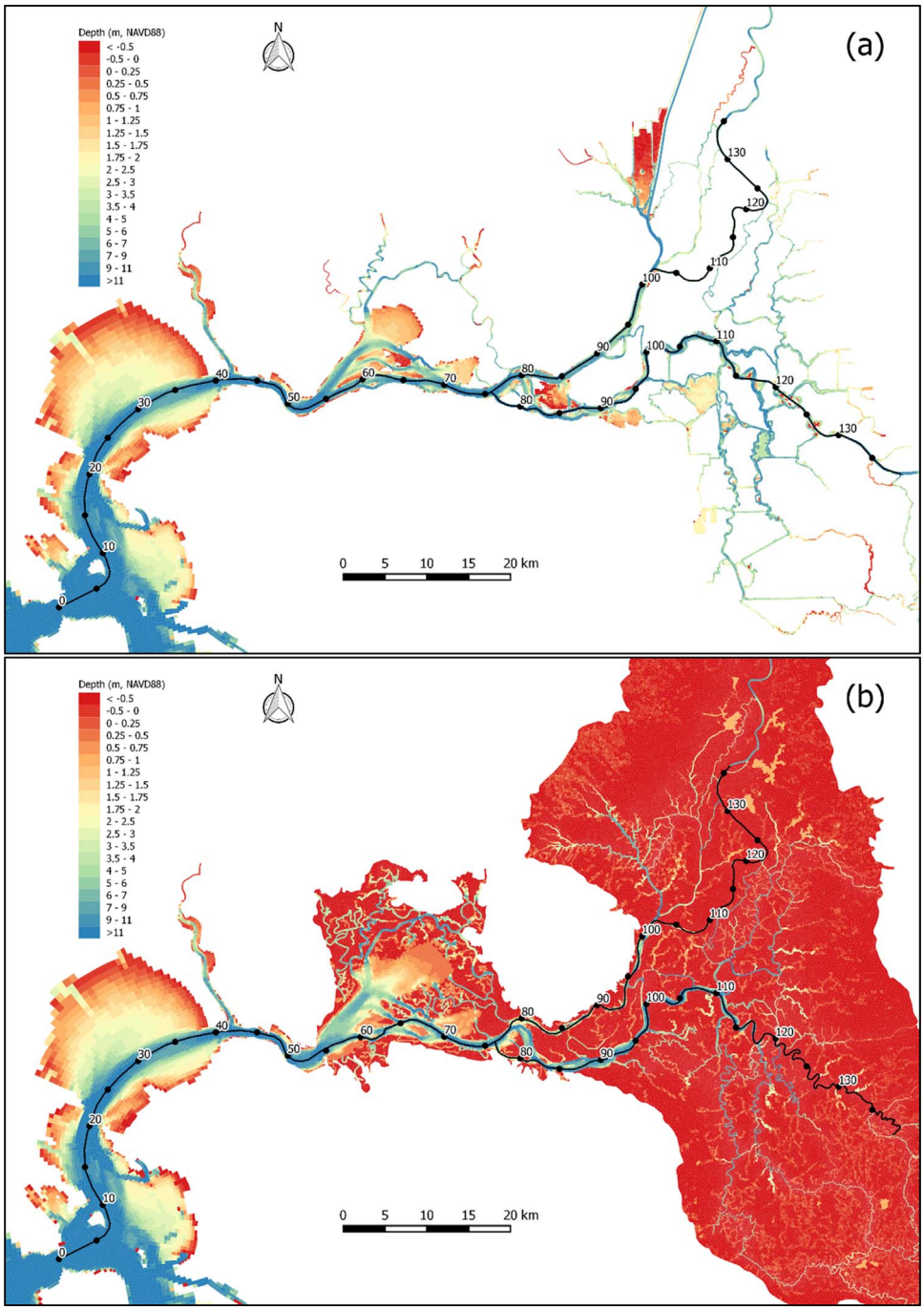

Fig. 5. (a) Contemporary and (b) pre-development isohaline transect locations. Transect distances are given in km. The more sinuous pre-development transect is scaled so that distances to corresponding geographical locations in the contemporary transect have the same values.

estuary is $\Delta F = F_{\text{in}} - F_{\text{out}}$.

Following MacCready (2011), flows and fluxes associated with only steady processes are derived from an Eulerian framework analysis and are labeled with the superscript Eu. They are defined as

$$Q^{\text{Eu}}(s) \equiv \int_{A_s^{Eu}} \langle u \rangle \langle dA \rangle, \qquad F^{\text{Eu}}(s) \equiv \int_{A_s^{Eu}} \langle s \rangle \langle u \rangle \langle dA \rangle \tag{11}$$

where A_s^{Eu} is the cross sectional area having tidally averaged salinity greater than s. Inflowing and outflowing Eulerian components are de fined similarly to Eq. (10). The flux analysis was performed on con temporary and pre development model results extracted at a cross section near Martinez (Fig. 1). This location was chosen because of its position at the seaward end of the upper estuary and because differ ences in channel characteristics (the pre development channel is wider and shallower here) are representative of general differences between the two systems.

Because our focus is on dispersive salt fluxes acting to transport salt into the upper estuary, the advective outflux of salt, $F_{\text{riv}} \equiv -Q_{\text{riv}} s_{\text{avg}}$, where s_{avg} is the tidally and cross sectionally averaged salinity, is re moved from the net fluxes. F_{riv} includes fluxes associated with both net estuary outflow and variation in the volume of the upper estuary due to spring neap tidal cycles, barometric pressure, and wind. In addition, flows calculated in the Eulerian reference frame will not include Stokes drift (an inflow to the estuary resulting from correlations between tidal velocity and depth), but will include the effect of Stokes compensation flow (a subtidal outflow). The salt flux associated with Stokes com pensation flow is estimated as

$$F_{\text{sdc}} \equiv \langle u'A' \rangle s_{\text{avg}} = [\langle uA \rangle - \langle u \rangle \langle A \rangle] s_{\text{avg}} = [Q_{\text{riv}} - (Q_{\text{in}}^{\text{Eu}} - Q_{\text{out}}^{\text{Eu}})] s_{\text{avg}} \tag{12}$$

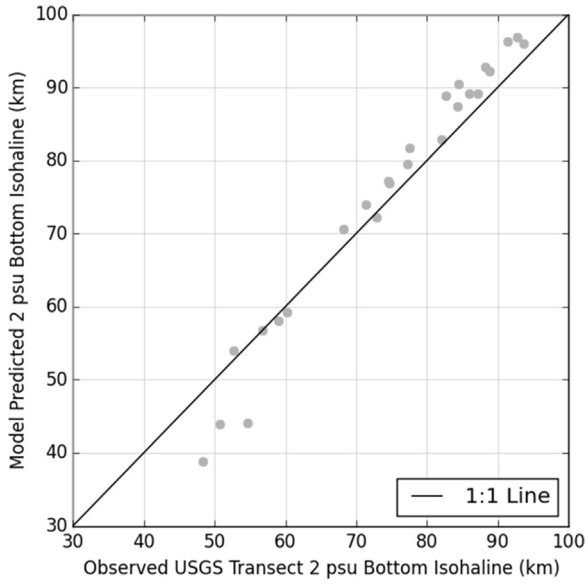

Fig. 6. Comparison of observed and model predicted 2 psu bottom isohaline location ("instantaneous" X2). Observed values are based on USGS transect data. Model predicted values are from the contemporary system simulation.

and removed from the net Eulerian flux calculation. The total dispersive salt fluxes, F_{disp}, can then be decomposed into steady and unsteady components as

$$\underbrace{\Delta F - F_{riv}}_{\text{total dispersive fluxes } (F_{disp})} = \underbrace{\Delta F^{Eu} - F_{riv} - F_{sdc}}_{\text{steady Eulerian fluxes } (F_{steady})} + \underbrace{F_{tid}}_{\text{unsteady tidal fluxes}} \quad (13)$$

In steady, estuarine exchange flow dominated systems, the total dispersive fluxes are expected to approximately equal the Eulerian es timate, $F_{disp} \approx F_{steady}$ (Chen et al., 2012). In tidal exchange dominated systems, the Eulerian flux will be small compared to the total, and $F_{disp} \approx F_{tid}$.

4. Results

4.1. Contemporary and pre development model calibrations

Fig. 6 compares USGS transect based X2 to "instantaneous" X2 (as opposed to the daily averaged X2) as simulated by the contemporary San Francisco Estuary model. The contemporary model accurately predicts X2 for the majority of the simulation period. The coefficient of determination (R^2), standard error, and mean absolute error of the model predictions were 0.977, 0.04 km, and 3.5 km, respectively. The highest model errors occurred during the period of very high flow at the beginning of 2006. During this time, stratification was generally under predicted by the model, leading to X2 farther seaward than observed.

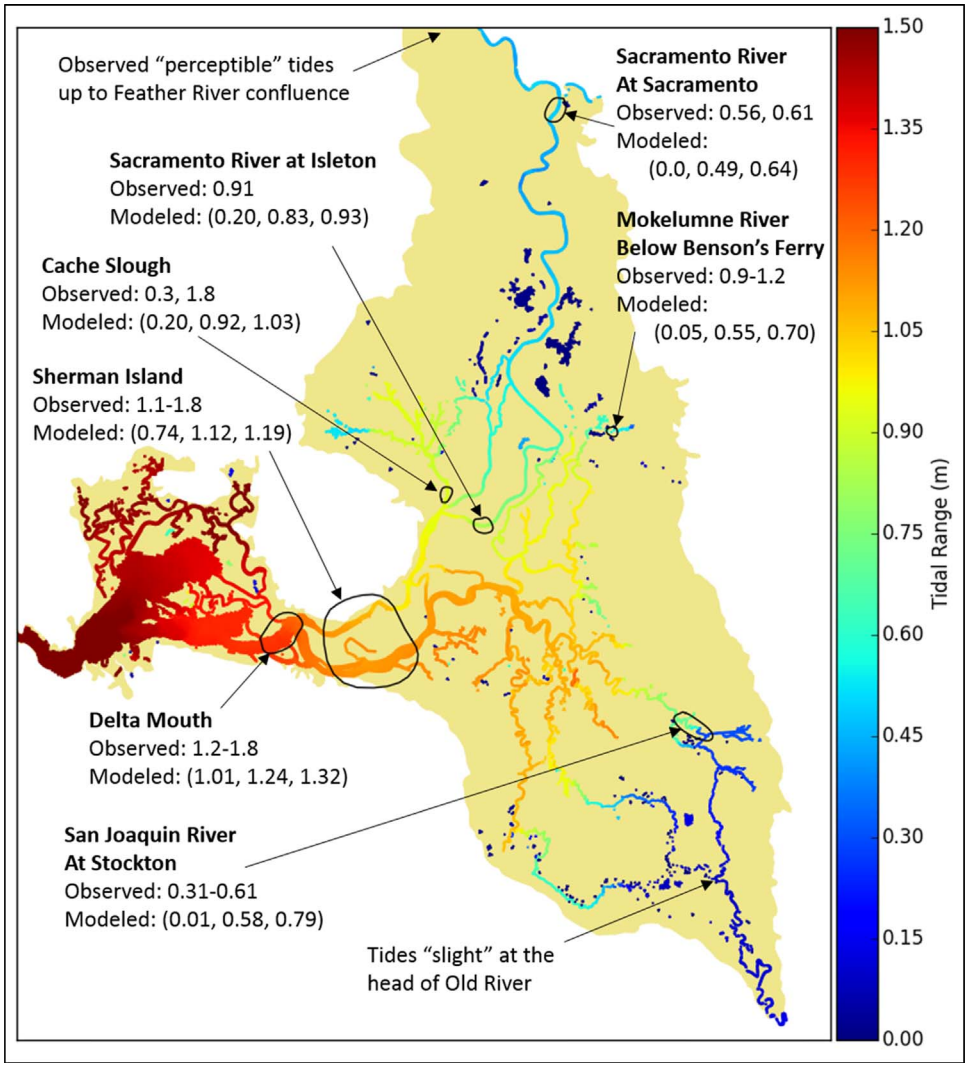

Fig. 7. Tidal range in the pre-development upper San Francisco Estuary. Historical observations are given along with the general area where the observation was made. The corresponding modeled values are given as the (minimum, median, maximum) monthly tidal ranges over the three-year simulation period. Areas with an average water depth less than 50 cm are shown as beige.

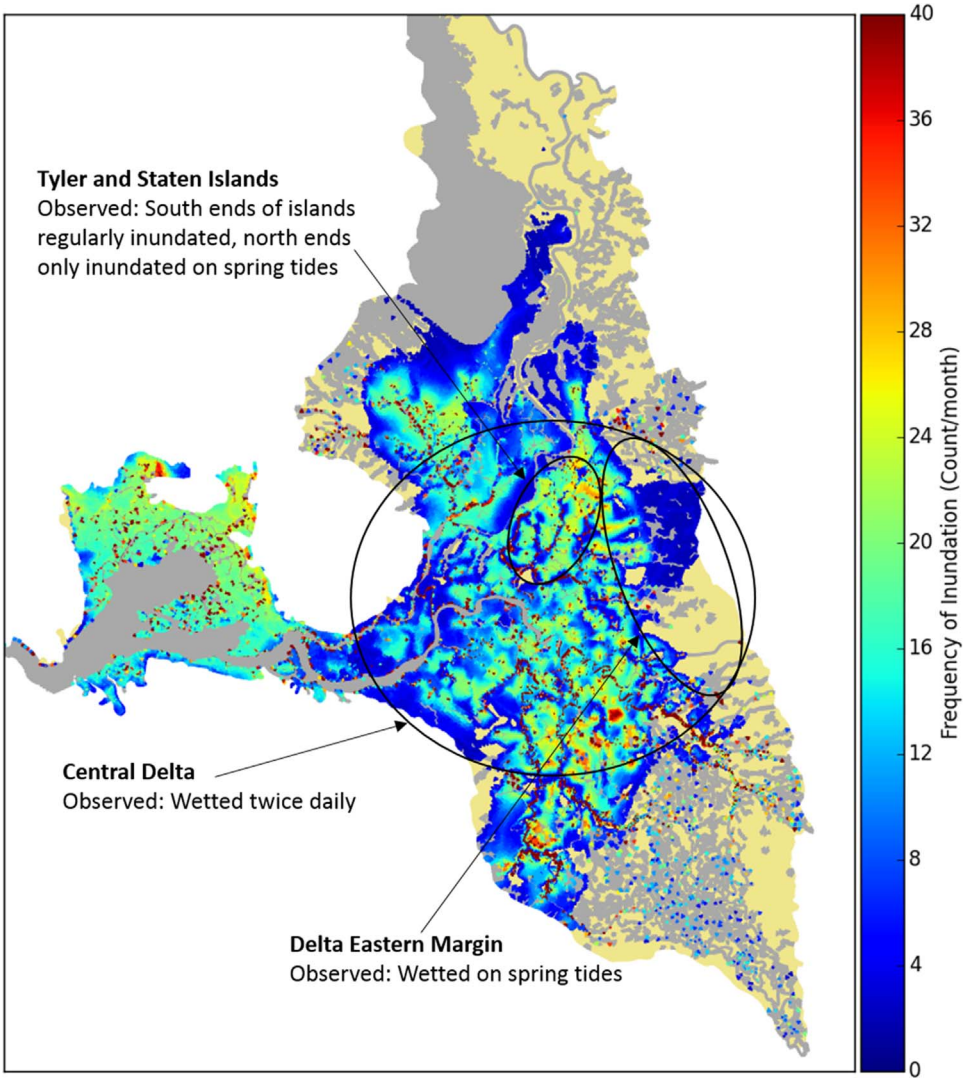

Fig. 8. Inundation frequency in the pre-development upper San Francisco Estuary. Historical observations are given along with the general area where the observation was made. The corresponding modeled values are the median of monthly inundation frequencies for months with maximum net estuary outflow less than 1000 $m^3 s^{-1}$. Areas which remain dry are shown as beige. Areas which remain wet are shown as gray.

Additional information on the contemporary San Francisco Estuary model calibration is provided in Appendix B, including comparisons of modeled and observed stage, flow, and salinity at continuous monitoring locations and USGS transect locations.

Historically observed channel tidal ranges are compared with the pre development model simulation in Fig. 7. The median monthly modeled tidal ranges generally matched or were slightly below historical observations at major locations in the Delta, including the Delta mouth, the Sacramento River at Isleton and the city of Sacramento, the Mokelumne River at Benson's Ferry, and the San Joaquin River at Stockton. The large difference between modeled and historically observed values at Cache Slough probably results from an incorrect observed value; it is unlikely that the pre development tidal range would be approximately twice as large as that observed at the nearby Isleton location. In the upper reaches of the estuary, tidal range varied significantly at a seasonal time scale. On the Sacramento River at Sacramento and the San Joaquin River at Stockton, tidal ranges were low during periods of high inflow. Range increased in the early summer when river stages were still relatively high and then decreased during the low flow fall period.

Historically observed inundation frequency is compared with the pre development model simulation in Fig. 8. In the pre development simulation, the majority of the central Delta is inundated 15 30 times per month. An inundation frequency of 30 times per month corresponds to marsh plain flooding during higher high tides; a frequency of 15 times a month corresponds to inundation only on higher high tide during spring tides. Inundation frequency in the interior of the marshes of the central Delta is generally greater than on the periphery of the marshes, as small natural levees cause flooding on lower high tide to occur through the heads of sloughs. The spatial extent of predicted tidal habitat in Fig. 8 generally matched that delimited by Whipple et al. (2012), shown in Fig. 3. The central Delta was dominated by tidal influence, but tidal habitat did not extend as far south along Old and Middle River, and extended farther on the eastern margin of the Delta than what was delimited.

Modeled tidal inundation depths (Fig. 9) were similar to some historical observations and lower than others. However, the observed data were scarce, often imprecise, and dependent on local topography. Less emphasis was therefore given to matching inundations depths in favor of the more precise historical observations of tidal range and inundation frequency.

A final aspect of the pre development Delta hydrodynamics examined during calibration was the flow patterns of marsh plain inundation and draining. At higher high tide, marsh plain was typically inundated from all directions as water spilled over low natural levees (Whipple et al., 2012). At lower high tide, marsh plain inundation occurred from spillover from the heads of blind sloughs that enter the plain from off the main channels. Marsh draining typically occurred back through the heads of these sloughs. Inclusion of the low natural levees fringing central Delta islands in the DEM allowed the modeled

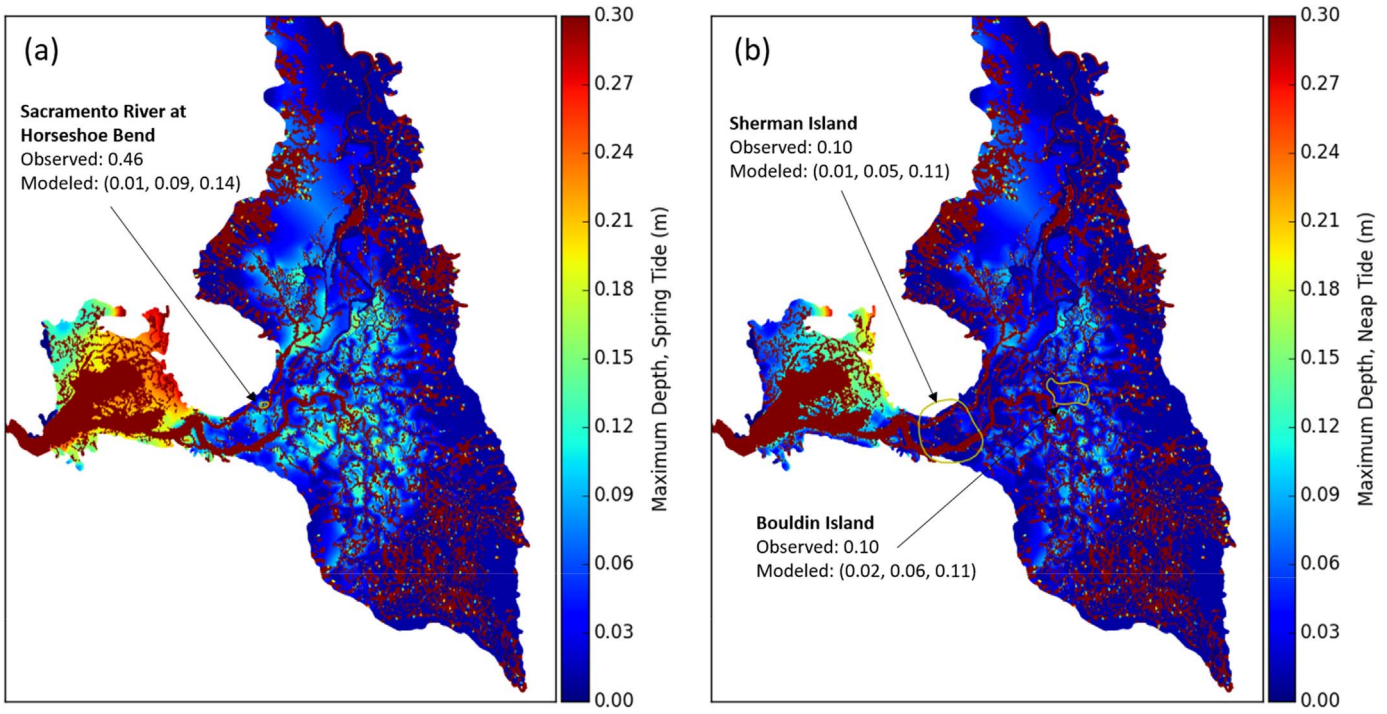

Fig. 9. Marsh plain inundation depths for spring tide periods (a) and neap tide periods (b) in the pre-development upper San Francisco Estuary. Historical observations are given along with the general area where the observation was made. The corresponding modeled values are given as the (minimum, median, maximum) of monthly inundation depths for months with maximum net estuary outflow less than 1000 $m^3 s^{-1}$.

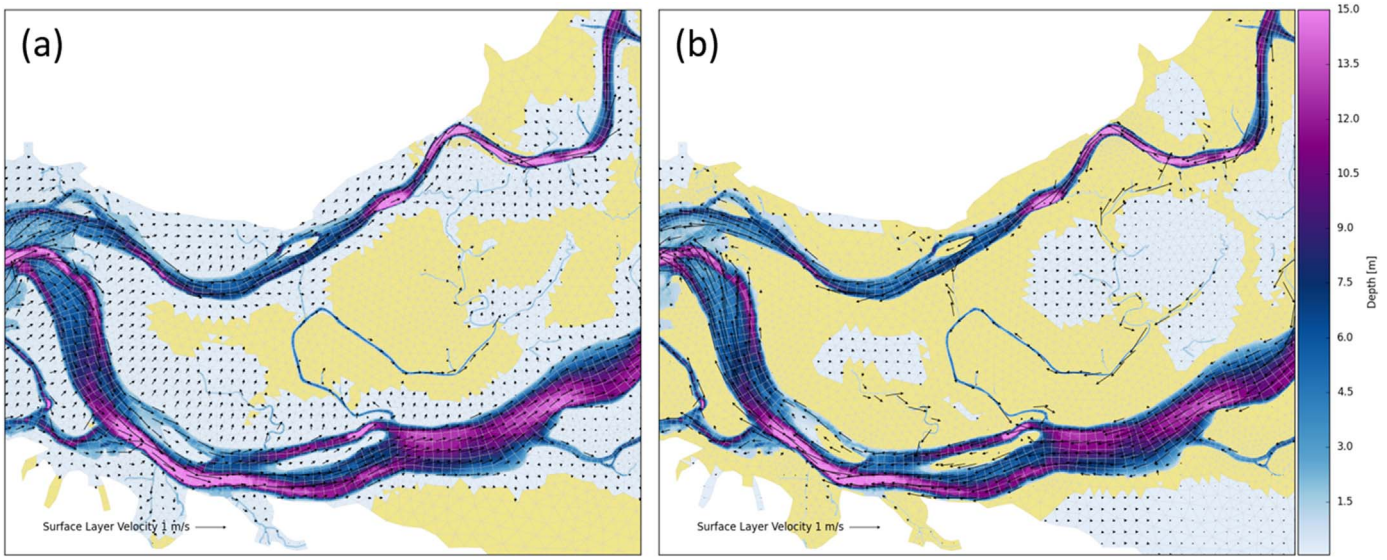

Fig. 10. (a) Marsh plain filling and (b) draining patterns in the pre-development simulation near Sherman Island. Dry areas are shown as beige. Modeled velocities were interpolated onto a coarser grid for visualization purposes.

tidal inundation flow patterns to generally reflect these trends (Fig. 10).

4.2. Salt intrusion length

The relationship between antecedent flow and X2, as predicted by the contemporary system model and by Eq. (5), is shown in Fig. 11a. The standard error of the regression fit is 1.70 km, and the coefficient of determination (R^2) is 0.986. The estimated γ is -0.230, which is identical to the value reported by MacWilliams et al. (2015) based on 3 D model simulations spanning the years 1994 1997. Similarly, the flow salinity relationship as predicted by the pre development system model and by Eq. (5) is shown in Fig. 11b. The standard error of the regression fit is 2.26 km, the coefficient of determination is 0.985, and the estimated γ is -0.237. Table 1 lists fit parameters and error metrics for each system model.

γ quantifies the system's response to changes in antecedent outflow; higher absolute values indicate a greater distance response. γ was slightly more negative for the pre development system than for the contemporary system, indicating the pre development salinity regime was slightly more sensitive to changes in outflow. Using a Student's t test, the difference in γ between the pre development and con temporary results was significant at the $p \leq 0.05$ level.

The parameter β_G (Eq. (6)) quantifies the system time response to changes in estuary outflow; higher values indicate a slower response. As

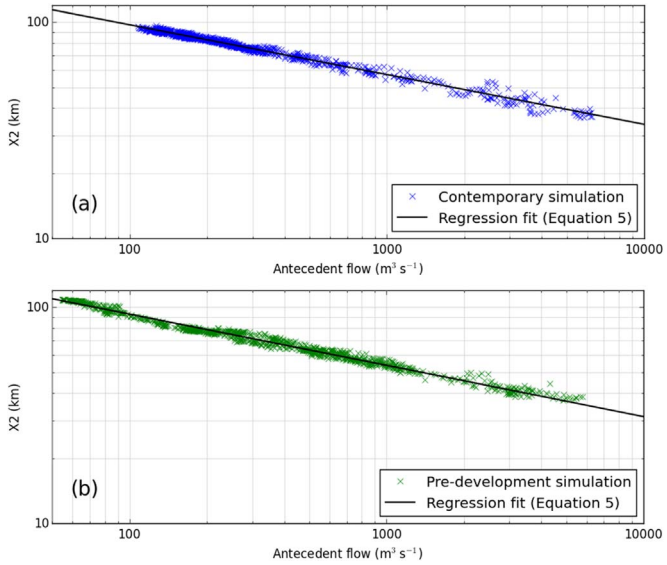

Fig. 11. X2 regression fits (Eq. (5)) for the contemporary (a) and pre-development (b) model simulations.

Table 1
X2 regression fit parameter values and error statistics. Parameters are defined in Eqs. (5) and (6).

Parameter	Scenario	
	Contemporary	Pre-development
β	281	277
γ	0.230	0.237
β_G ($m^3 s^{-1} day$)	5739	4458
Standard error (km)	1.70	2.26
R^2	0.986	0.985

shown in Table 1, β_G was lower for the pre development system than for the contemporary system. This suggests that, for a given antecedent flow, the pre development system responded faster to changes in net estuary outflow. However, as shown in Fig. 12, the antecedent flow also varies substantially between pre development and contemporary sys tems, due to different seasonal timing of outflow.

Fig. 12 compares contemporary and pre development model cal culated outflow, antecedent flow (Eq. (6)), X2 (Eq. (5)), and the ad justment time scale of salinity to flow (Eq. (7)). Differences in the time series largely reflect differences in estuary outflow. Similar outflows through much of 2006 led to similar X2. Much larger differences were seen in late 2006 through 2008, where higher pre development system outflows in winter and spring resulted in X2 10 20 km seaward of the contemporary system. Lower pre development outflows in summer and fall resulted in X2 10 20 km landward of the contemporary system. The adjustment time is not only a function of β_G but also inversely related to antecedent flow. Thus despite the lower β_G for the pre development estuary, the longest adjustment times occur for pre development con ditions.

Two key differences between the pre development and con temporary model scenarios influence salinity predictions: the time history of estuary outflow and the estuary's geometry and bathymetry. To isolate the influence of changes to the estuary's geometry and bathymetry, the fitting parameters listed in Table 1 were used to gen erate X2 time series for each system assuming identical outflow time series. The results are shown for contemporary simulation outflows in Fig. 13a and pre development simulation outflows in Fig. 13b. The predicted X2 values were generally similar given the same outflows. The mean absolute difference in X2 was 3.23 km and 90% of the differences were within 4.68 km. For a given antecedent flow, X2 is located farther seaward in the pre development system than in the contemporary system. A higher steady outflow is therefore required for the contemporary system to obtain the same X2 as in the pre devel opment system. For X2 in the range 50 110 km, the outflows required to obtain the same X2 are 28% higher, on average, in the contemporary system.

4.3. Salt intrusion mechanisms

Total exchange flow and the associated salt fluxes and flux weighted salinities calculated for the contemporary estuary simulation are shown in Fig. 14. After a period of high flow in the spring of 2006, the total exchange flow remains relatively steady and is typically 3 4 times higher than the net estuary outflow, Q_{riv}. Increases in both Q_{in} and Q_{out} occur during spring tide conditions (Fig. 14a). For low and moderate net estuary outflows, Q_{in} reaches a peak during spring tides which is approximately double the minimum during neap tide. In Fig. 14, the timing of peak spring tides is indicated with background vertical lines. This was done to indicate changes in variables with the strength of the tides when viewing the plots. Peak spring tide conditions were de termined by finding the local maxima in the root mean square tidal flow time series, Q_{rms}, computed by applying a 30 h moving window root mean square to the flow time series at Martinez.

Both inflowing and outflowing salinity decrease with net estuary outflow (Fig. 14b). Similar to the exchange flow, model predicted salinity typically increases during spring tides. Tidally averaged strati fication, Δs, is relatively less variable than inflowing and outflowing salinity, and generally increases during neap tides and periods of higher flow.

The calculated total incoming salt flux component (F_{in}) is roughly balanced by the outgoing salt flux (F_{out}), indicating gradual changes in salt mass landward of Martinez (Fig. 14c). Increased net estuary out flow decreases both flux components due to the effect of outflow on salinity. The calculated Eulerian flux components are not in balance because they do not represent salt transport due to Stokes drift but do include transport from Stokes drift compensation flow.

Advective salt fluxes from the estuary mirror the short term changes in net flow past the cross section (Q_{riv}) resulting from variability in water storage in Suisun Bay and the Delta (Fig. 14d). Water storage, as indicated by subtidal water levels in the upper estuary, has been re ported to vary with the spring neap cycle, barometric pressure, and wind stress (Andrews et al., 2016; Monismith, 2016). Since we are more interested in net salt transport mechanisms than variability due to changes in water storage, we remove the salt fluxes associated with net flow from the total and Eulerian flux estimates (Eq. (13)). From the Eulerian estimate, we also remove Stokes drift compensation flow, and the resulting landward salt flux is referred to as the *steady Eulerian flux* (F_{steady}). It is associated with estuarine circulation and other processes that influence tidally averaged velocity and salinity correlations. The remaining landward salt flux is referred to as *tidal flux* (F_{tid}), consistent with the terminology in Chen et al. (2012), and is associated with subtidal salt flux associated with tidal trapping and other tidally un steady processes. These unsteady tidal fluxes are found to contribute more to the net salt influx at this location than steady Eulerian fluxes (Fig. 14e). As expected, tidal salt fluxes increase during spring tides, whereas steady fluxes increase during neap tides.

Steady Eulerian salt fluxes account for a greater percentage of the total in the contemporary simulation (long term average 36%) than the pre development simulation (long term average 21%; see Fig. 15). This is likely a result of a deeper channel at Martinez and through Suisun Bay in the contemporary system increasing the potential for estuarine circulation. The contemporary system also shows greater spring neap variability in the partitioning between steady and unsteady fluxes. During neap tides, 50 60% of the total dispersive flux is Eulerian while during spring tides only 20 30% is. The Eulerian contribution in the

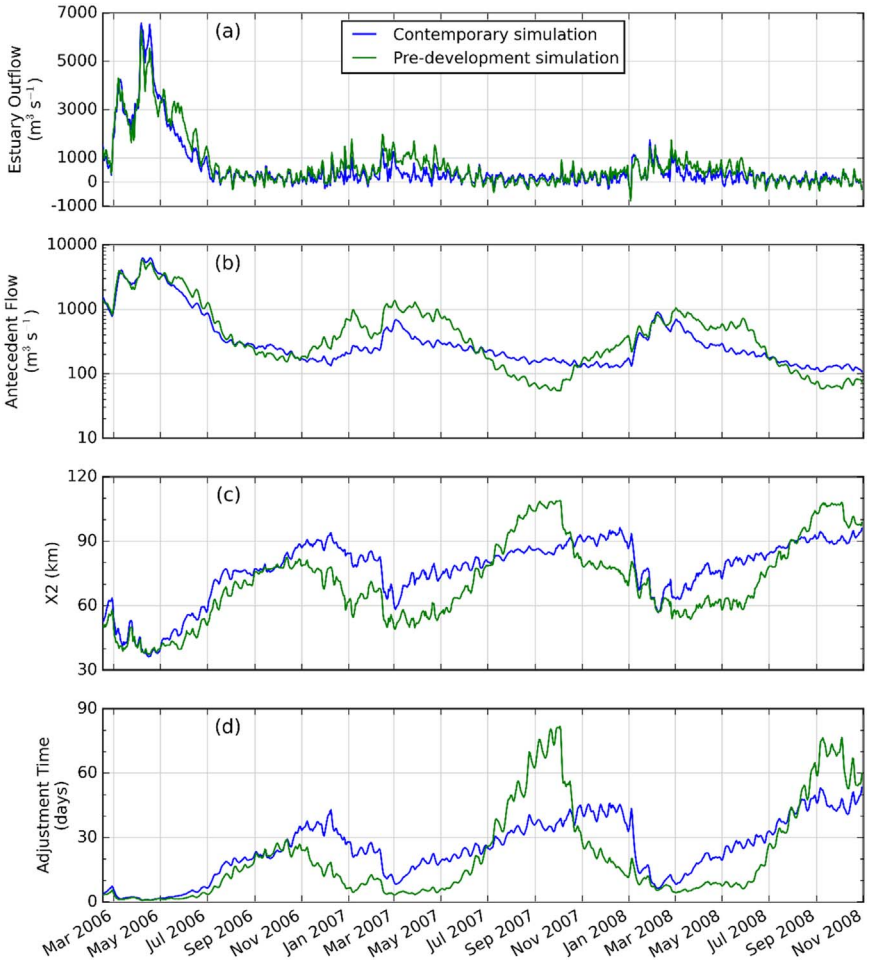

Fig. 12. (a) Model calculated net estuary outflow, (b) antecedent flow, (c) X2, and (d) adjustment time for the contemporary and pre-development estuary simulations.

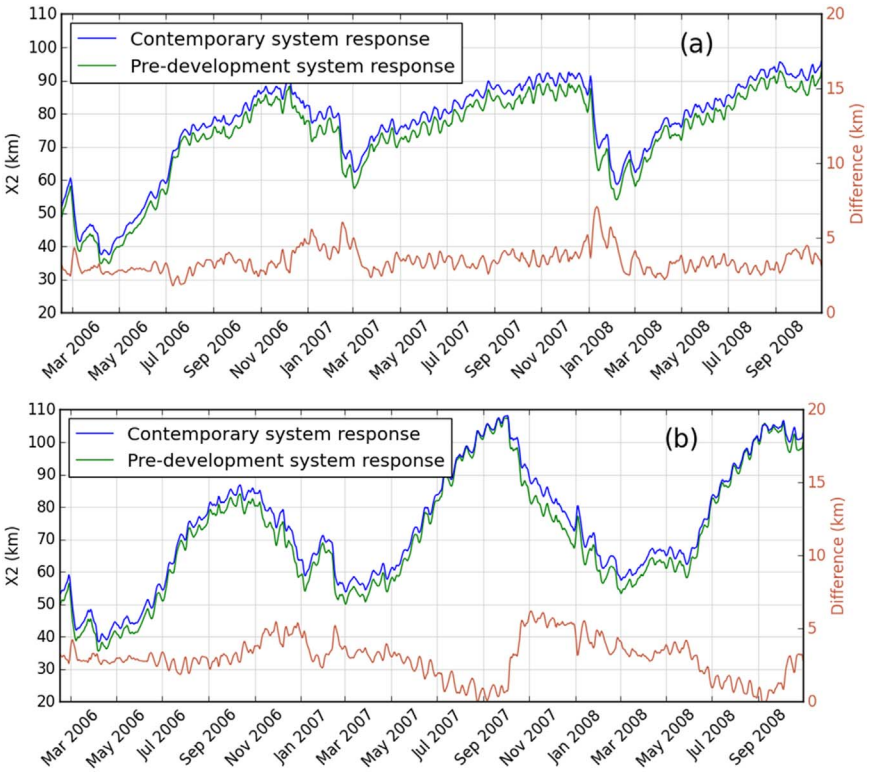

Fig. 13. X2 in the contemporary estuary and pre-development estuary for (a) the contemporary estuary outflow and (b) pre-development net Delta outflow. Secondary axis shows difference in X2.

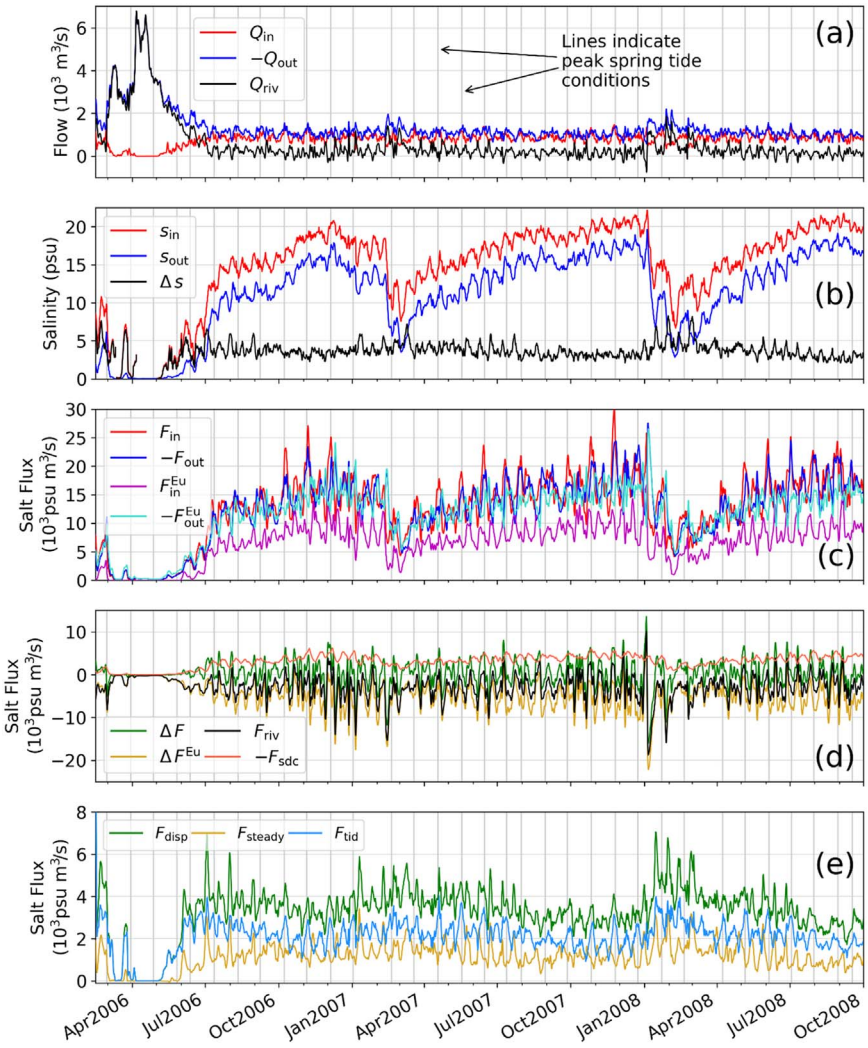

Fig. 14. Contemporary estuary simulation (a) total exchange flows, (b) exchange flow salinities, (c) isohaline derived salt fluxes, (d) net isohaline salt fluxes, along with river and Stokes drift compensation flow fluxes, and (e) total dispersive salt fluxes, broken into steady and unsteady contributions. In all plots, vertical gray lines indicate peak spring tide conditions.

pre development simulation is more constant, typically varying 10 30%.

5. Discussion

Calibration of the pre development model was limited by a lack of historical observations and the approximate nature of many of these observations. Topography and bathymetry measurements were sparse and entirely absent in many regions, which limits confidence that the exact conditions of the pre development system were reproduced. Given this limited data availability, approximations were necessary to represent some landscape features (e.g., use of a simplified prescription of a planar regional marsh plain elevation) and some processes were ignored (e.g., explicit surface water groundwater interaction). Despite these limitations, the pre development model contains the salient fea tures of the system numerous blind sloughs, sinuous channels, and broadly inundated marshland and is useful for comparison with the modified environment of the contemporary estuary.

The simulated pre development and contemporary estuary outflows were substantially different, with pre development outflows being higher in winter and spring and lower in summer and fall. These flow differences resulted in substantial salt intrusion length differences. Inter and intra annual variability in X2 were both greater in the pre development simulations. To isolate the influence of changes to the estuary's geometry and bathymetry, the response of both systems to the same outflow time series was compared. Differences in salt intrusion length due to changes in bathymetry were found to be relatively small (Fig. 13) despite the dramatic modifications that have taken place since the mid 19th century. The X2 model parameters β and γ (Eq. (5)) are similar for both systems, indicating roughly the same salt intrusion length for the same antecedent flow. The parameter β_G (Eq. (6)) is substantially smaller for the pre development system (4458 m^3 s^{-1} day) relative to the contemporary system (5739 m^3 s^{-1} day), indicating faster response of salinity to changes in flows under pre development conditions for a given antecedent flow. The larger range of flows during pre development conditions leads to more variable adjustment time and higher maxima during the lowest flow conditions.

Many studies have estimated the power dependence of X2 to out flow, γ, for the San Francisco Estuary. Values range from a low de pendence on outflow of -0.143 (Monismith et al., 2002) to a higher dependence of -0.230 (MacWilliams et al., 2015). The range in these estimates may be attributed to the data source (surface or bottom fixed salinity monitoring stations, numerical model results) and time period used for the regression, the parameterization of the response time coefficient (α), as well as the specifics of the regression analysis. Bias in the calculation of γ can result from using surface salinity stations and an assumed level of stratification, as well as not allowing α to vary in time (MacWilliams et al., 2015). 3 D numerical models may over estimate vertical mixing at high outflows (Chua and Fringer, 2011), resulting in underestimations of X2 at high flows and biasing the cal culation of γ. Our result for the contemporary San Francisco Estuary ($\gamma = -0.230$) is on the high range of the estimates, but is comparable to

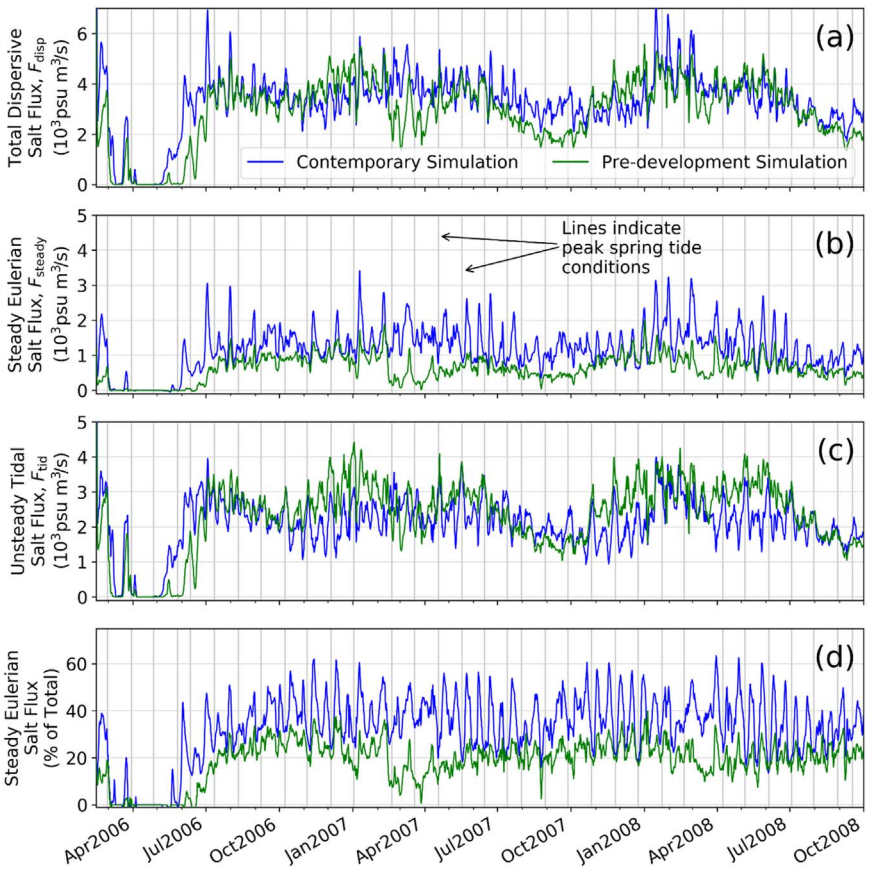

Fig. 15. Contemporary and pre-development simulation dispersive salt fluxes: (a) total fluxes, (b) steady Eulerian fluxes, (c) unsteady tidal fluxes, (d) steady fluxes as a percent of total. In all plots, vertical gray lines indicate peak spring tide conditions.

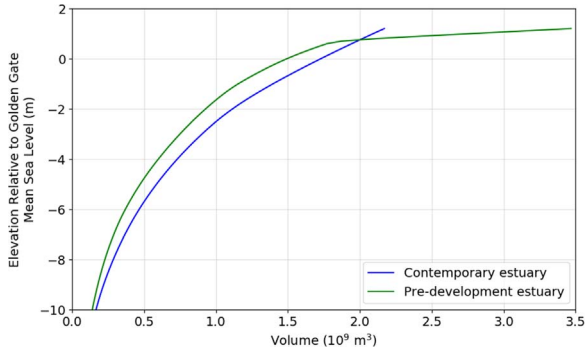

Fig. 16. Hypsographic curves of the contemporary and pre-development upper San Francisco Estuary.

other studies using numerical modeling results (Gross et al., 2009; Hutton, 2014; MacWilliams et al., 2015).

In the analytical analysis of Hansen and Rattray (1965), γ was derived as $-1/3$. MacCready (1999) reported that while the expected value for estuarine circulation dominated estuaries is $-1/3$, a value of -1 is expected for dispersion dominated estuaries. All studies of the San Francisco Estuary show a lower sensitivity of X2 to outflow than theoretical predictions suggest. Monismith et al. (2002) concluded the deviation is due to the geometry of the estuary, which is not represented in the analytical analysis, and the effects of stratification on vertical mixing, which were neglected in Hansen and Rattray (1965). They hypothesized that during high flows and neap tides, the estuary switches from one in which SIPS dominates to a state where stratification increases with time, causing non linear increases in salt fluxes up estuary. Our analysis is consistent with this explanation, with the highest steady salt fluxes associated with high flow and neap tides. The capacity for this process is dampened in the shallower pre development system, and may contribute to the higher outflow response coefficient ($= -0.237$) than was found for the contemporary system.

Recent research by Chen (2015) suggests that, for the same net outflow, the salinity field adjusts faster when flow is increasing than when it is decreasing. By specifying the response time scale as a function of antecedent flow ($\tau = \beta_G/Q_{ant}$), our method is consistent with this finding. Since antecedent flow can be converted to a salt intrusion length (Eq. (5)), our work is also consistent with Monismith (2017), which specified the response time scale as a function of salt intrusion length (X2).

It should be noted how successful these simple regression models are at reproducing their respective datasets. For example, the model used in this study (Hutton et al., 2015) consists of only three empirical parameters and one input (estuary outflow) yet reproduces modeled X2 over a wide range of flow conditions with the high degree of accuracy for both the pre development and contemporary San Francisco Estuary systems. In other systems, strong variability of salt intrusion length occurs over the spring neap cycle, with longer intrusion length during neap tides due to variability in vertical mixing (Ralston et al., 2008). This variability is ignored in our analysis, as minimal spring neap X2 variability is predicted in the hydrodynamic model simulations. In addition, several physical processes which influence salt intrusion for example, coastal sea level (Walters and Gartner, 1985) and wind (Walters et al., 1985) are ignored by the simple X2 model, yet a standard error of 1.70 km and a coefficient of determination of 0.986 are achieved for the contemporary system.

Fig. 14e suggests a potential explanation for the muted spring neap variation in X2 found in the estuary: the importance of both steady estuarine circulation processes and unsteady tidal processes in bringing salt into the estuary. While tidal processes are stronger on spring tides, estuarine circulation is stronger on neap tides, moderating large swings in salt intrusion length. In the pre development system, unsteady tidal

processes make up a larger portion of dispersive fluxes than in the contemporary system. This is consistent with the analysis of Chen et al. (2012), which indicated that the importance of steady fluxes relative to unsteady fluxes is expected to increase with water depth, because the strength of estuarine circulation increases with depth.

The shallower channels of the pre development system may also be the cause for differences in the X2 regression parameters between the systems. Hypsographic curves of the two systems are shown in Fig. 16. The contemporary estuary has more volume at most elevations in the upper estuary because of deeper channels dredged for shipping and several flooded islands. These features are absent in the pre development system, but a rapid expansion in volume is seen above mean high water because of extensive marsh plains. From a purely advective point of view, a system with similar planform geometry but less volume would respond more quickly to changes in flow, and for a given flow, salinity would intrude less than a system with more volume. Both of these conclusions were noted in our regression analysis for the pre development system.

Despite differences in flows and stratification, dispersive tidal fluxes up estuary are similar in the two simulations for much of the year (Fig. 15). While the shallower channels of the pre development system result in weaker steady exchange flow, such as estuarine circulation processes, unsteady tidal fluxes are higher. The more complex and sinuous channel network in Suisun Marsh may result in enhanced tidal trapping bringing salt and material into the estuary. This difference in transport mechanisms has implications for the transport of materials that are not uniformly distributed in the vertical. Estuarine circulation preferentially transports negatively buoyant material up estuary near the bed. This includes sediment (Schoellhamer, 2001) and is also hypothesized to influence recruitment of negatively buoyant or downward swimming organisms from the ocean to more productive low salinity habitat (Kimmerer, 2002). In contrast, unsteady tidal processes transport material uniformly in the vertical.

Channel deepening due to sea level rise and dredging maintenance of the shipping channels are expected to enhance estuarine circulation processes in the future San Francisco Estuary. The addition (re introduction) of large areas of tidal marsh in Suisun Marsh for restoration has the potential to increase tidal trapping processes. While both of these changes to the estuary could potentially increase the strength of dispersive salt flux mechanisms, the comparison of pre development and contemporary systems suggests that increases in the strength of one salt intrusion from a change in estuary geometry can be partially offset by decreases in the strength of other salt intrusion processes. The estimated change in the total strength of dispersive flux was found to be limited, but salt intrusion length differed substantially between the pre development and contemporary estuary due to differences in net estuary outflow.

6. Summary

Extensive anthropogenic modifications of the San Francisco Estuary and its watershed have occurred since the mid 19th century. These modifications have influenced both hydrology in the watershed and salt transport mechanisms in the estuary. Previous studies (Fox et al., 2015; CDWR, 2016f) have estimated changes in hydrology. This work explores the changes in salt intrusion resulting from both the altered inflow hydrology and estuarine geometry.

Three dimensional hydrodynamic models were developed to quantitatively assess differences in salt intrusion between the San Francisco Estuary under contemporary and pre development conditions. Results from the contemporary model calibration indicate that the modeling framework is sufficient to accurately predict water level, flow, and salinity in the estuary. The pre development system model was calibrated by varying marsh plain elevations in order to match sparse observations of tidal characteristics. A recent three year period covering a range of flow conditions was used to compare the hydrodynamic behavior of the two systems. While the contemporary model simulation assumed historical observed boundary conditions, the pre development model simulation assumed conditions thought to exist prior to the alterations of the past two centuries.

Following the approach of Hutton et al. (2015), relationships between net estuary outflow and the longitudinal distance from the estuary mouth to the 2 psu bottom salinity isohaline (X2) were developed for each system. This fitting approach involves only three empirical parameters and was found to reliably capture the variability in X2 predicted by the three dimensional hydrodynamic model of each system. This approach is also consistent with recent findings that the system time scale of adjustment is directly related to salt intrusion length (Monismith, 2017).

Salt intrusion in the pre development estuary was found to be slightly more sensitive to outflow and responded faster to changes in outflow than in the contemporary estuary. Changes in hydrology associated with the stabilizing effect of contemporary water management on outflow were responsible for more of the salt intrusion differences between the two systems than were changes in estuary geometry and bathymetry.

Tidal trapping and other unsteady salt intrusion processes were found to be more important in the pre development estuary than in the contemporary one. In both systems, steady processes such as estuarine circulation were strongest during neap tides and unsteady salt intrusion processes were strongest during spring tides, resulting in limited spring neap variability in salt intrusion. Expected future changes to the estuary include sea level rise which is likely to increase the strength of estuarine circulation and large scale restoration which is likely to increase the strength of tidal trapping. However, given that multiple physical mechanisms are important for salt intrusion in the upper San Francisco Estuary, future increases in the strength of one mechanism may be partially offset with decreases in the strength of another.

Finally, a key product of this work is a set of calibrated 3 D hydrodynamic models for the pre development and contemporary San Francisco Estuary. We hope that these tools will be useful to researchers and estuary managers in future investigations into aspects of both systems.

Acknowledgments

The authors wish to thank all the members of the pre development San Francisco Estuary modeling team, including William Fleenor, Andy Bell, and Alison Whipple (University of California, Davis); Sam Safran and Robin Grossinger (San Francisco Estuary Institute); Tariq Kadir and Guobiao Huang (CDWR); and John DeGeorge, Stacie Grinbergs, and Richard Rachiele (Resource Management Associates). We also thank Steve Micko (UC Davis) for his work on hydraulic structures in the contemporary estuary model. Finally, we wish to acknowledge the contributions of Eli Ateljevich (CDWR), Christoph Lippert (Smile Consult), Stefan Talke and Hamed Moftakhari Rostamkhani (University of California, Irvine), and Rusty Holleman (SFEI) for sharing their expertise in specific aspects of the modeling methods and analysis. This work was supported by Metropolitan Water District of Southern California. Additional support for Edward Gross was provided by the Center for Watershed Sciences, UC Davis. The manuscript was significantly improved by the comments from Stephen Monismith (Stanford University) and an anonymous reviewer.

Appendix A. Historical observations

Historical observed data for comparison with model output are shown in Table A.1. Data extracted from the historical accounts are generally uncertain as the exact location of the measurement, and observations are typically rough estimates. An example of a relatively precise observation is an account from a farmer at Horseshoe Bend on the Sacramento River that his two and one half foot high levee was "about one foot above the spring tide mark," meaning that the pre leveed marsh was likely inundated by a foot and a half of water at spring tides (Higley, 1860). An example of a less precise observation was made by a visitor to Stockton, who noted "the tide of the ocean and Bay of San Francisco, sets up here, from one to two feet" (McCollum, 1850).

Table A.1
Quantitative historical observations of tidal characteristics in the Delta, from Whipple et al. (2012).
Source: Source publication year is not necessarily indicative of the year the observation was taken.

Observation Type	Value	Location	Source
Tidal range in channel	perceptible	Sacramento River at Feather River confluence	Sacramento Daily Union (1862)
Tidal range in channel	0.56 m, 0.61 m	Sacramento River at Sacramento	Sacramento Daily Union (1862), McCollum (1850)
Tidal range in channel	0.9 m (regular), 1.2 m (spring)	Mokelumne River below Benson's Ferry	Thayer (1955), Payson (1885), Thornton (1859)
Tidal range in channel	0.91 m (post hydraulic mining debris)	Sacramento River at Isleton	Hall (1879)
Tidal range in channel	1.8 m (low-water), 0.3 m (flood stage)	Cache Slough	Rose et al. (1895)
Tidal range in channel	1.1–1.8 m	Sherman Island	Day (1869)
Tidal range in channel	1.2–1.8 m	Delta mouth	Abella and Cook (1960), Farnham (1857), Rose et al. (1895)
Tidal range in channel	0.3–0.61 m, 0.61 m	San Joaquin River at Stockton	McCollum (1850), Payson (1885)
Tidal range in channel	perceptible	San Joaquin River at head of Old River	Abella and Cook (1960)
Inundation frequency	south ends of islands regularly inundated, north ends only on spring tides	Tyler and Staten Islands	Thompson (2006)
Inundation frequency	"Wetted" twice daily	Central Delta	Whipple et al. (2012)
Inundation frequency	"Wetted" on spring tides	Eastern margin of Delta	Whipple et al. (2012)
Depth of marsh plain inundation	0.46 m (spring tide)	Sacramento River at Horseshoe Bend	Higley (1860)
Depth of marsh plain inundation	"Wetted", 0.15 m (neap tide)	Sherman Island	Rose et al. (1895), Day (1869)
Depth of marsh plain inundation	0.15 m	Bouldin Island	Beaumont (1861)

Appendix B. Contemporary San Francisco Estuary model calibration results

At each of the continuous monitoring stations shown in Fig. B.1, observed flow or stage data were compared against model predicted values on both tidal and tidally averaged time scales. Average computed minus observed values were calculated to assess tidally averaged errors. Tidal time scale error metrics included phase error (lag) and amplitude error. The coefficient of determination was calculated after correcting the modeled values for phase error, following the methods described in RMA (2005). A model skill metric (Willmott, 1981) was also computed.

Model flow and stage error metrics are given in Table B.1 and Table B.2. Of the 31 flow stations, 22 (71%) had model skill accuracies classified as *accurate* (> 0.975), using the category thresholds given by MacWilliams et al. (2015). Five stations (16%) had skill accuracies classified as *acceptable* (0.950 0.975), and four stations (13%) were classified as *poor agreement* (< 0.950). Of the four stations with poor agreement, two were located in the north Delta and resulted from inaccurate model flow splits through Sacramento River junctions; the other two were located in central Delta areas with complex flow geometries. Of the 48 stage stations, 25 (52%) had model skill accuracies classified as *accurate* (skill value cutoffs were the same as for flow). Eighteen stations were in the *acceptable* range (38%), and five stations (10%) were classified as *poor agreement*. Of the five stations with poor agreement, four had model skill values just below the *acceptable* classification cutoff (in the range 0.943 0.949). Amplitude ratios were generally above 1.0, indicating slight overestimation of tidal range. Computed stages were lower than observed on average.

USGS salinity transect comparisons are shown for the 25 cruises performed within the model simulation period in Fig. B.2. In each set of images, observed salinities are shown in the left subplot. Model results are shown for the corresponding times and locations on the right. Salinity contours are shown in intervals of 2 psu. The model is shown to accurately predict isohaline locations and stratification levels, except during times of very high flow when the stratification is underpredicted.

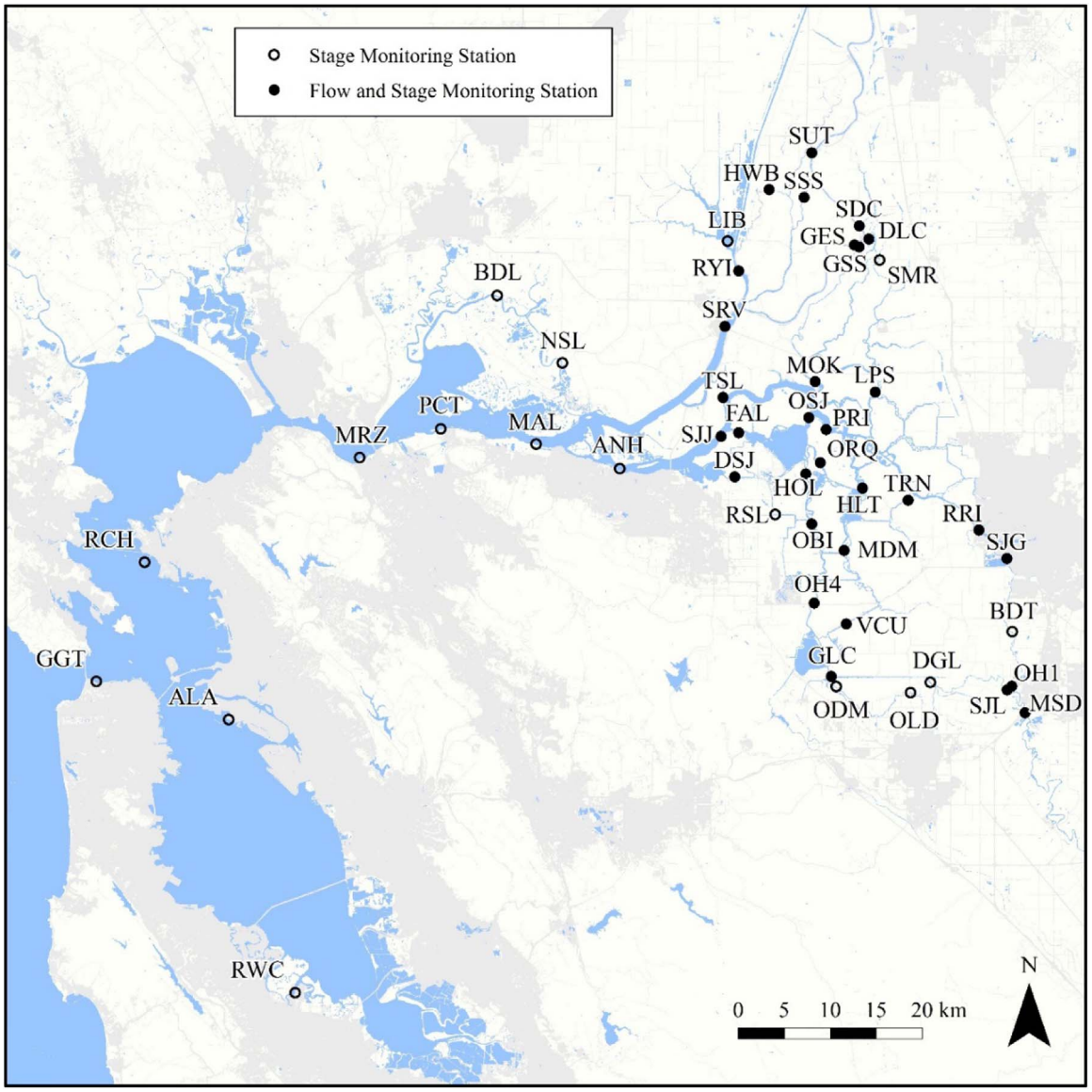

Fig. B.1. Continuous monitoring station locations for contemporary San Francisco Estuary model calibration.

Table B.1
Contemporary San Francisco Estuary model flow accuracy metrics. Skill classification is based on the thresholds given in MacWilliams et al. (2015).

Station Name	Station Abbrev.	Data Source	Average Observed ($m^3 s^{-1}$)	Average Computed ($m^3 s^{-1}$)	Computed – Observed ($m^3 s^{-1}$)	Lag (min)	Amplitude Ratio	R^2	Model Skill	Skill Class
Sacramento River at Rio Vista	SRV	USGS	417.6	434.9	17.3	−14	0.979	0.985	0.993	Accurate
Threemile Slough at San Joaquin River	TSL	USGS	−39.4	−33.8	5.6	7	1.127	0.981	0.990	Accurate
Cache Slough at Ryer Island	RYI	USGS	150.7	134.8	−15.9	−9	0.912	0.985	0.993	Accurate
Sacramento River below Georgiana Slough	GES	USGS	196.6	168.1	−28.5	−7	0.996	0.988	0.992	Accurate
Georgiana Slough at Sacramento River	GSS	USGS	106.4	144.6	38.2	−10	1.167	0.989	0.945	Poor agreement
Delta Cross Channel	DLC	USGS	56.4	46.0	−10.4	−27	0.826	0.967	0.971	Acceptable
Sacramento River above Delta Cross Channel	SDC	USGS	352.4	361.5	9.2	−4	1.119	0.991	0.997	Accurate
Sutter Slough at Courtland	SUT	USGS	98.3	78.1	−20.2	−26	1.682	0.881	0.944	Poor agreement
Steamboat Slough between Sacramento River and Sutter Slough	SSS	USGS	102.2	95.2	−7.0	−9	1.126	0.982	0.994	Accurate
Miner Slough at Hwy 84 Bridge	HWB	USGS	89.9	72.5	−17.4	−13	1.351	0.929	0.968	Acceptable
San Joaquin River at Jersey Point	SJJ	USGS	173.9	183.5	9.6	−10	0.944	0.980	0.993	Accurate
False River near Oakley	FAL	USGS	−27.0	37.4	64.4	0	1.096	0.981	0.992	Accurate
Mokelumne River at San Joaquin River	MOK	USGS	94.4	114.1	19.7	−5	1.008	0.978	0.993	Accurate
Little Potato Slough at Terminous	LPS	USGS	54.6	60.6	6.0	−7	0.915	0.954	0.986	Accurate
San Joaquin River at Prisoners Point	PRI	USGS	−106.9	−27.4	79.5	−22	0.875	0.971	0.979	Accurate
Old River at Franks Tract	OSJ	USGS	−10.6	−61.0	−50.4	29	0.560	0.763	0.853	Poor agreement
Dutch Slough at Jersey Island	DSJ	USGS	−0.4	−0.7	−0.2	−13	0.997	0.968	0.988	Accurate
Holland Cut near Bethel Island	HOL	USGS	−29.9	−30.1	−0.2	−11	0.905	0.973	0.989	Accurate
Old River at Quimby Island	ORQ	USGS	−36.4	−39.3	−2.9	0	1.018	0.973	0.993	Accurate
Middle River near Holt	HLT	USGS	−72.8	−56.4	16.4	−15	0.929	0.965	0.986	Accurate
Turner Cut near Holt	TRN	USGS	−29.0	−37.2	−8.1	−7	0.586	0.896	0.913	Poor agreement
Old River at Bacon Island	OBI	USGS	−38.8	−33.4	5.4	−18	0.866	0.971	0.982	Accurate
Middle River at Middle River	MDM	USGS	−74.5	−83.7	−9.2	−14	0.893	0.963	0.985	Accurate
Old River at Hwy 4	OH4	USGS	−79.1	−80.0	−1.0	−8	0.898	0.941	0.984	Accurate
Victoria Canal near Byron	VCU	USGS	−44.5	−41.5	3.1	−13	0.705	0.866	0.953	Acceptable
Grant Line Canal near Tracy	GLC	USGS	48.9	50.5	1.6	−21	0.847	0.889	0.963	Acceptable
San Joaquin River at Rough and Ready Island	RRI	CDWR	27.4	20.0	−7.5	−13	0.766	0.902	0.956	Acceptable
San Joaquin River at Garwood Bridge	SJG	USGS	52.0	54.4	2.4	−15	0.861	0.979	0.992	Accurate
San Joaquin River below Old River near Lathrop	SJL	CDWR	43.3	50.1	6.8	−1	0.867	0.974	0.989	Accurate
Old River at Head	OH1	CDWR	69.5	55.8	−13.7	−12	0.620	0.983	0.976	Accurate
San Joaquin River at Mossdale Bridge	MSD	CDWR	112.6	112.8	0.2	−24	0.675	0.994	0.998	Accurate

Table B.2
Contemporary San Francisco Estuary model stage accuracy metrics. Skill classification is based on the thresholds given in MacWilliams et al. (2015). USGS stations indicated with an asterisk have stage measured relative to an arbitrary vertical datum and were shifted to match average computed values at that location.

Station Name	Station Abbrev.	Data Source	Average Observed (m)	Average Computed (m)	Computed – Observed (m)	Lag (min)	Amplitude Ratio	R^2	Model Skill	Skill Class
San Francisco at Golden Gate	GGT	NOAA	0.957	0.939	−0.018	4	1.005	0.995	0.998	Accurate
Alameda	ALA	NOAA	0.959	0.973	0.014	13	0.995	0.995	0.997	Accurate
Redwood City	RWC	NOAA	1.002	1.002	0.000	20	0.967	0.993	0.992	Accurate
Richmond	RCH	NOAA	0.967	0.973	0.005	5	0.995	0.996	0.999	Accurate
Martinez	MRZ	CDWR	1.126	1.065	−0.061	3	0.991	0.967	0.988	Accurate
Port Chicago	PCT	NOAA	1.131	1.111	−0.020	8	0.972	0.982	0.994	Accurate
Sacramento River at Mallard Island	MAL	CDWR	1.210	1.169	−0.041	12	0.961	0.973	0.989	Accurate
Montezuma Slough at National Steel	NSL	CDWR	1.207	1.129	−0.078	4	1.176	0.969	0.980	Accurate
Montezuma Slough at Beldons Landing	BDL	CDWR	1.139	1.130	−0.009	0	0.980	0.949	0.987	Accurate
Sacramento River at Antioch	ANH	CDWR	1.306	1.200	−0.106	17	1.008	0.969	0.970	Acceptable
Sacramento River at Rio Vista	SRV	USGS	1.278	1.175	−0.103	12	1.078	0.972	0.969	Acceptable
Threemile Slough at San Joaquin River	TSL	USGS	1.355	1.205	−0.150	1	1.085	0.970	0.954	Acceptable
Cache Slough at Ryer Island	RYI	USGS	1.316	1.211	−0.105	−2	1.096	0.974	0.975	Acceptable
Liberty Island at south end	LIB	USGS	1.391	1.228	−0.164	3	1.049	0.910	0.943	Poor agreement
Sacramento River below Georgiana Slough	GES	USGS	1.633	1.516	−0.117	1	1.118	0.987	0.986	Accurate
Georgiana Slough at Sacramento River	GSS	USGS	1.617	1.494	−0.123	−1	1.132	0.983	0.983	Accurate
Delta Cross Channel	DLC	USGS	1.436	1.322	−0.114	1	1.161	0.935	0.958	Acceptable
South Fork Mokelumne River	SMR	USGS	1.414	1.311	−0.103	10	1.119	0.964	0.969	Acceptable
Sacramento River above Delta Cross Channel	SDC	USGS	1.683	1.547	−0.136	−4	1.144	0.987	0.984	Accurate
Sutter Slough at Courtland	SUT	USGS	1.678	1.455	−0.223	−15	1.224	0.951	0.915	Poor agreement
Steamboat Slough between Sacramento River and Sutter Slough	SSS	USGS	1.675	1.519	−0.156	−5	1.163	0.978	0.975	Acceptable
Miner Slough at Hwy 84 Bridge	HWB	USGS	1.537	1.365	−0.171	−17	1.224	0.928	0.947	Poor agreement
San Joaquin River at Jersey Point	SJJ	USGS	1.256	1.181	−0.075	9	1.061	0.967	0.978	Accurate
*False River near Oakley	FAL	USGS	1.127	1.129	0.002	34	1.051	0.943	0.973	Acceptable
*Mokelumne River at San Joaquin River	MOK	USGS	1.176	1.170	−0.006	1	1.091	0.966	0.990	Accurate
*Little Potato Slough at Terminous	LPS	USGS	1.190	1.189	−0.001	1	1.083	0.970	0.991	Accurate
*San Joaquin River at Prisoners Point	PRI	USGS	1.158	1.158	0.000	26	1.067	0.937	0.976	Accurate
*Old River at Franks Tract	OSJ	USGS	1.177	1.177	0.000	1	1.089	0.967	0.990	Accurate
Dutch Slough at Jersey Island	DSJ	USGS	1.257	1.181	−0.076	−7	1.074	0.943	0.972	Acceptable
*Holland Cut near Bethel Island	HOL	USGS	1.162	1.161	0.000	−4	1.092	0.964	0.989	Accurate
Rock Slough	RSL	CDWR	1.334	1.192	−0.142	−8	1.062	0.937	0.946	Poor agreement
*Old River at Quimby Island	ORQ	USGS	1.162	1.160	−0.002	22	1.072	0.936	0.977	Accurate
*Middle River near Holt	HLT	USGS	1.170	1.171	0.001	2	1.078	0.966	0.990	Accurate
*Turner Cut near Holt	TRN	USGS	1.178	1.176	−0.002	23	1.050	0.936	0.977	Accurate
Old River at Bacon Island	OBI	USGS	1.318	1.195	−0.123	4	1.076	0.966	0.960	Acceptable
Middle River at Middle River	MDM	USGS	1.336	1.195	−0.141	−5	1.079	0.968	0.952	Acceptable
Old River at Hwy 4	OH4	USGS	1.257	1.156	−0.101	−10	1.072	0.960	0.968	Acceptable
Old River at Delta Mendota Canal	ODM	USGS	1.254	1.259	0.005	−17	1.025	0.837	0.949	Poor agreement
Old River near Tracy	OLD	CDWR	1.339	1.328	−0.011	4	1.037	0.902	0.968	Acceptable
Doughty Cut above Grant Line Canal	DGL	CDWR	1.340	1.353	0.013	−6	1.064	0.942	0.983	Accurate
*Victoria Canal near Byron	VCU	USGS	1.137	1.138	0.001	−5	1.059	0.960	0.988	Accurate
Grant Line Canal near Tracy	GLC	USGS	1.179	1.077	−0.103	−5	1.037	0.920	0.959	Acceptable
San Joaquin River at Rough and Ready Island	RRI	CDWR	1.333	1.218	−0.115	6	1.050	0.967	0.968	Acceptable
San Joaquin River at Garwood Bridge	SJG	USGS	1.350	1.254	−0.096	−8	1.101	0.961	0.975	Acceptable
San Joaquin River at Brandt Bridge	BDT	CDWR	1.577	1.398	−0.179	−13	1.208	0.956	0.961	Acceptable
San Joaquin River below Old River near Lathrop	SJL	CDWR	1.751	1.808	0.057	−5	1.062	0.990	0.992	Accurate
Old River at Head	OH1	CDWR	1.375	1.403	0.028	−4	−1.000	0.882	0.964	Acceptable
San Joaquin River at Mossdale Bridge	MSD	CDWR	1.932	2.038	0.106	7	1.017	0.991	0.991	Accurate

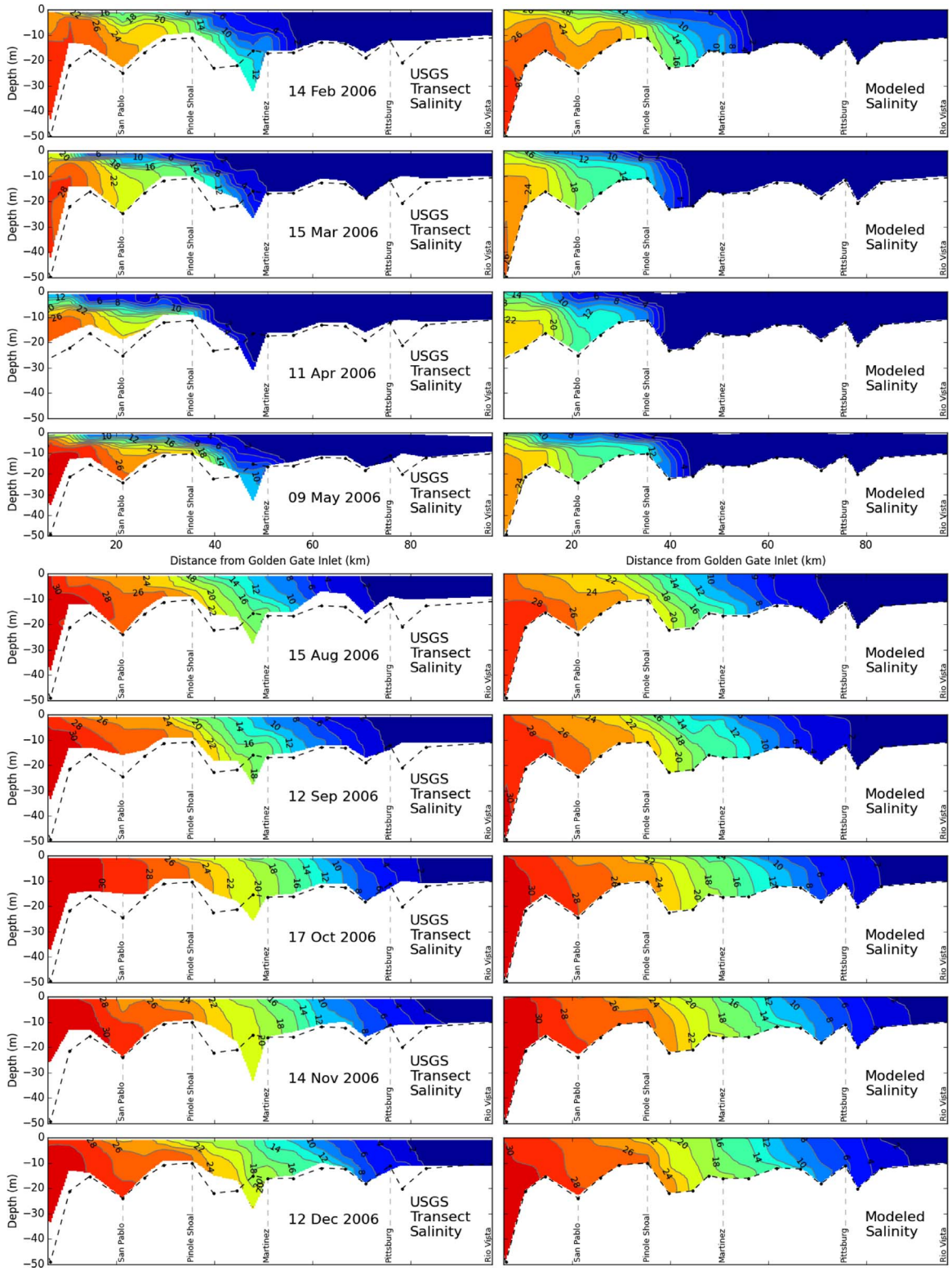

Fig. B.2. USGS Polaris cruise measured (left column) and model results (right column). Black dotted lines indicate model bathymetry along transect.

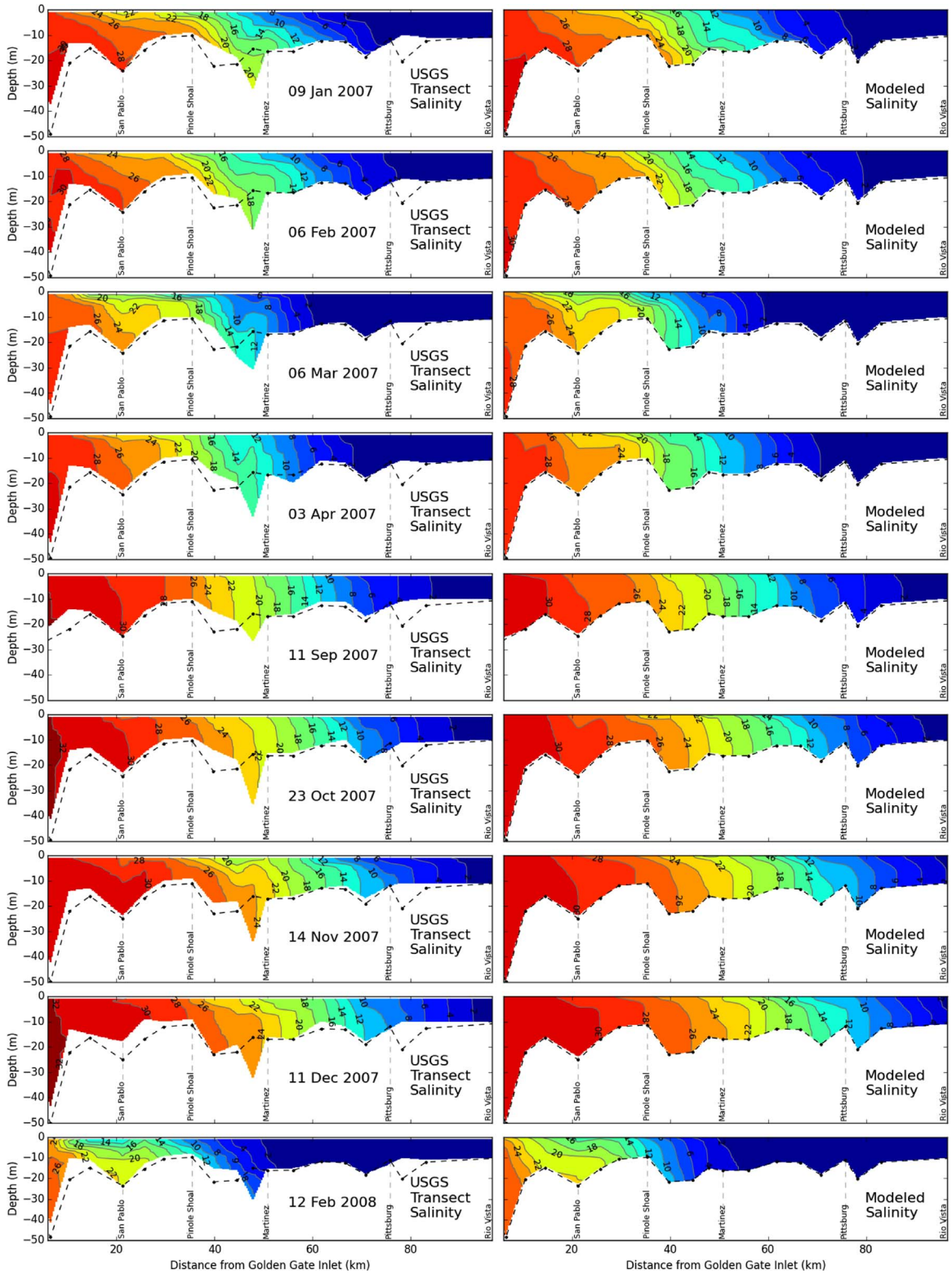

Fig. B.2. (*continued*)

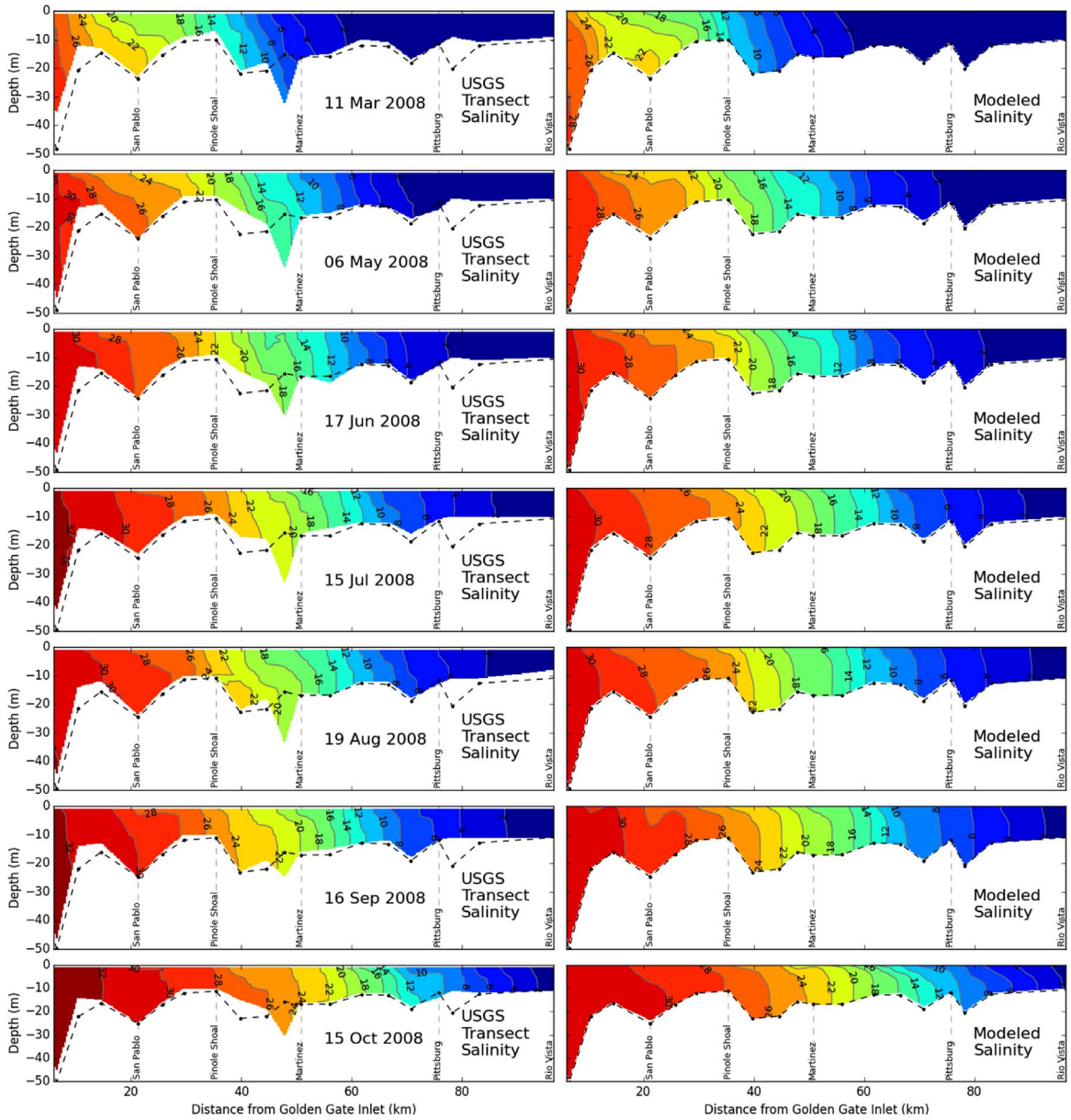

Fig. B.2. (*continued*)

References

Abella, R., Cook, S.F., 1960. Colonial Expeditions to the Interior of California Central Valley, 1800–1820. University of California Press, Berkeley, California, USA.

Andrews, S.W., Gross, E.S., Hutton, P.H., 2016. A water balance model to estimate flow through the Old and Middle River corridor. San Franc. Estuary Watershed Sci. 14 (2). ⟨http://escholarship.org/uc/item/8c5574hf⟩.

Atwater, B.F., Conard, S.G., Dowden, J.N., Hedel, C.W., MacDonald, R.L., Savage, W., 1979. History, landforms, and vegetation of the estuary's tidal marshes. In: Conomos, T.J. (Ed.), San Francisco Bay: The Urbanized Estuary. Pacific Division. American Association for the Advancement of Science, San Francisco, California, USA, pp. 347–385.

Barnard, P.L., Foxgrover, A.C., Elias, E.P.L., Erikson, L.H., Hein, J.R., McGann, M., Mizell, K., Rosenbauer, R.J., Swarzenski, P.W., Takesue, R.K., Wong, F.L., Woodrow, D.L., 2013. Integration of bed characteristics, geochemical tracers, current measurements, and numerical modeling for assessing the provenance of beach sand in the San Francisco Bay coastal system. Mar. Geol. 336, 120–145. http://dx.doi.org/10.1016/j.margeo.2012.11.008.

Beaumont, D., California State Land Office, 1861. Swamp and Overflowed Lands Reports and Correspondence. Box 44. Courtesy of California State Archives, Sacramento, California, USA.

[CSWRCB] California State Water Resources Control Board, 1999. Revised Water Right Decision 1641 in the Matter of: Implementation of Water Quality Objectives for the San Francisco Bay/Sacramento-San Joaquin Delta Estuary. ⟨http://www.swrcb.ca.gov/waterrights/board decisions/adopted orders/decisions/d1600 d1649/wrd1641 1999dec29.pdf⟩. (Accessed 5 July 2016).

[CDWR] California Department of Water Resources, 2016a. California Data Exchange Center. ⟨http://cdec.water.ca.gov/index.html⟩. (Accessed 5 July 2016).

[CDWR] California Department of Water Resources, 2016b. California Irrigation Management Information System. ⟨http://www.cimis.water.ca.gov/⟩. (Accessed 5 July 2016).

[CDWR] California Department of Water Resources, 2016c. Chronological Reconstructed Sacramento and San Joaquin Valley Water Year Hydrological Classification Indices. ⟨http://cdec.water.ca.gov/cgi-progs/iodir/wsihist⟩. (Accessed 5 July 2016).

[CDWR] California Department of Water Resources, 2016d. Dayflow, An Estimate of Daily Average Delta Outflow. ⟨http://www.water.ca.gov/dayflow⟩. (Accessed 5 July 2016).

[CDWR] California Department of Water Resources, 2016e. Delta Simulation Model II – DSM2. ⟨http://baydeltaoffice.water.ca.gov/modeling/deltamodeling/models/dsm2/dsm2.cfm⟩. (Accessed 5 July 2016).

[CDWR] California Department of Water Resources, 2016f. Estimates of Natural and Unimpaired Flows for the Central Valley of California: Water Years 1922–2014. ⟨https://msb.water.ca.gov/documents/86728/a702a57f-ae7a-41a3-8bff-722e144059d6⟩. (Accessed 5 July 2016).

Casulli, V., 2009. A high-resolution wetting and drying algorithm for free-surface hydrodynamics. Int. J. Numer. Methods Fluids 60, 391–408. http://dx.doi.org/10.1002/fld.1896.

Casulli, V., Stelling, G.S., 2010. Semi-implicit subgrid modelling of three-dimensional free-surface flows. Int. J. Numer. Methods Fluids 67, 441–449. http://dx.doi.org/10.

1002/fld.2361.
Casulli, V., Walters, R.A., 2000. An unstructured grid, three-dimensional model based on the shallow water equations. Int. J. Numer. Methods Fluids 32, 331–348. http://dx.doi.org/10.1002/(SICI)1097-0363(20000215)32:3< 331::AID-FLD941> 3.0.CO;2-C.
Casulli, V., Zanolli, P., 2005. High resolution methods for multidimensional advection-diffusion problems in free-surface hydrodynamics. Ocean Model. 10, 137–151. http://dx.doi.org/10.1016/j.ocemod.2004.06.007.
Chen, S.N., 2015. Asymmetric estuarine responses to changes in river forcing: a consequence of nonlinear salt flux. J. Phys. Ocean. 45, 2836–2847. http://dx.doi.org/10.1175/JPO-D-15-0085.1.
Chen, S.N., Geyer, W.R., Ralston, D.K., Lerczak, J.A., 2012. Estuarine exchange flow quantified with isohaline coordinates: contrasting long and short estuaries. J. Phys. Oceanogr. 42, 748–763. http://dx.doi.org/10.1175/JPO-D-11-086.1.
Cheng, R.T., Casulli, V., Gartner, J.W., 1993. Tidal, residual, intertidal mudflat (TRIM) model and its application to San Francisco Bay, California. Estuar. Coast. Shelf Sci. 36, 235–280. http://dx.doi.org/10.1006/ecss.1993.1016.
Chua, V.P., Fringer, O.B., 2011. Sensitivity analysis of three-dimensional salinity simulations in North San Francisco Bay using the unstructured-grid SUNTANS model. Ocean Model. 39, 332–350. http://dx.doi.org/10.1016/j.ocemod.2011.05.007.
Conomos, T.J., 1979. Properties and circulation of San Francisco Bay waters. In: Conomos, T.J. (Ed.), San Francisco Bay: The Urbanized Estuary. Pacific Division. American Association for the Advancement of Science, San Francisco, California, USA, pp. 47–84.
Day, S., 1869. Report of Sherman Day, Surveyor-General. In: Fresh water tide lands of California. M. D. Carr & Co.
Denton, R.A., 1993. Accounting for antecedent conditions in seawater intrusion modeling—applications for the San Francisco Bay–Delta. In: Shen, H.W., Su, S.T., Wen, F. (Eds.), Hydraulic Engineering 1993. American Society of Civil Engineers, pp. 448–453.
Farnham, J.T., 1960. Life, Adventure and Travels in California. Sheldon, Blakeman & Co., New York.
Fischer, H.B., List, E.J., Koh, R.C.Y., Imberger, J., Brooks, N.H., 1979. Mixing in Inland and Coastal Waters. Academic Press, New York.
Fox, J.P., Mongan, T.R., Miller, W.J., 1990. Trends in freshwater inflow to San Francisco Bay from the Sacramento–San Joaquin Delta. J. Am. Water Resour. Assoc. 26 (1), 101–116. http://dx.doi.org/10.1111/j.1752-1688.1990.tb01355.x.
Fox, P., Hutton, P.H., Howes, D.J., Draper, A.J., Sears, L., 2015. Reconstructing the natural hydrology of the San Francisco Bay-Delta watershed. Hydrol. Earth Syst. Sci. 19, 4257–4274. http://dx.doi.org/10.5194/hess-19-4257-2015.
Fram, J.P., Martin, M.A., Stacey, M.T., 2007. Dispersive fluxes between the coastal ocean and a semienclosed estuarine basin. J. Phys. Oceanogr. 37 (6), 1645–1660. http://dx.doi.org/10.1175/JPO3078.1.
Geyer, W.R., MacCready, P., 2014. The estuarine circulation. Annu. Rev. Fluid Mech. 46 (1), 175–197. http://dx.doi.org/10.1146/annurev-fluid-010313-141302.
Gross, E.S., MacWilliams, M.L., Kimmerer, W.J., 2009. Three-dimensional modeling of tidal hydrodynamics in the San Francisco Estuary. San Franc. Estuary Watershed Sci. 7 (2). 〈http://escholarship.org/uc/item/9rv243mg〉.
Hall, W.H., 1879. William Hammond Hall Collection, Field Books, Box 3, Book 45, 8–32. Courtesy of California State Archives, Sacramento, California, USA.
Hansen, D.V., Rattray Jr., M., 1965. Gravitational circulation in straits and estuaries. J. Mar. Res. 23, 104–122.
Higley, H.A., 1860. Annual Report of the Surveyor-General for the Year 1860. State Land Office.
Howes, D.J., Fox, P., Hutton, P.H., 2015. Evapotranspiration from natural vegetation in the Central Valley of California: monthly grass reference-based vegetation coefficients and the dual crop coefficient approach. J. Hydrol. Eng. ASCE 20 (10), 04015004. http://dx.doi.org/10.1061/(ASCE)HE.1943-5584.0001162.
Hutton, P.H., 2014. Delta Salinity Gradient (DSG) Model. Internal Report. Metropolitan Water District of Southern California. Sacramento, California, USA. pp. 1–209. 〈http://www.baydeltalive.com/docs/10000〉. (Accessed 5 July 2016).
Hutton, P.H., Rath, J.S., Chen, L., Ungs, M.J., Roy, S.B., 2015. Nine decades of salinity observations in the San Francisco Bay and Delta: modeling and trend evaluation. ASCE J. Water Resour. Plan. Manag. 142. http://dx.doi.org/10.1061/(ASCE)WR.1943-5452.0000617.
Hyatt, E., 1931. Variation and control of salinity in the Sacramento–San Joaquin Delta and Upper San Francisco Bay. California Department of Public Works, Sacramento, California, USA. pp. 1–440.
Jassby, A.D., Kimmerer, W.J., Monismith, S.G., Armor, C., Cloern, J.E., Powell, T.M., Schubel, J.R., Vendlinski, T.J., 1995. Isohaline position as a habitat indicator for estuarine populations. Ecol. Appl. 5, 272–289. http://dx.doi.org/10.2307/1942069.
Kimmerer, W.J., 2002. Effects of freshwater flow on abundance of estuarine organisms: physical effects or trophic linkages? Mar. Ecol. Prog. Ser. 243, 39–55. http://dx.doi.org/10.3354/meps243039.
Kimmerer, W.J., 2004. Open water processes of the San Francisco Estuary: from physical forcing to biological responses. San Franc. Estuary Watershed Sci. 2 (1). http://escholarship.org/uc/item/9bp499mv.
Kimmerer, W.J., Gross, E.S., MacWilliams, M.J., 2009. Variation of physical habitat for estuarine nekton with freshwater flow in the San Francisco Estuary. Estuaries Coasts 32 (2), 375–389. http://dx.doi.org/10.1007/s12237-008-9124-x.
Kimmerer, W.J., MacWilliams, M.L., Gross, E.S., 2013. Variation of fish habitat and extent of the low salinity zone with freshwater flow in the San Francisco Estuary. San Franc. Estuary Watershed Sci. 11 (4). http://escholarship.org/uc/item/3pz7x1x8.
Lerczak, J.A., Geyer, W.R., 2004. Modeling the lateral circulation in straight, stratified estuaries. J. Phys. Oceanogr. 34, 1410–1428. http://dx.doi.org/10.1175/1520-0485(2004)034%3C1410:MTLCIS%3E2.0.CO;2.
Lerczak, H.A., Geyer, W.R., Ralston, D.K., 2009. The temporal response of the length of a partially stratified estuary to changes in river flow and tidal amplitude. J. Phys. Oceanogr. 39 (4), 915–933. http://dx.doi.org/10.1175/2008JPO3933.1.
Levenberg, K., 1944. A method for the solution of certain non-linear problems in least squares. Q. Appl. Math. 2, 164–168.
Lund, J., Hanak, E., Fleenor, W.E., Howitt, R., Mount, J., Moyle, P., 2007. Envisioning Futures for the Sacramento–San Joaquin Delta. Public Policy Institute of California, San Francisco, California, USA. http://www.ppic.org/main/publication.asp?i=671.
MacCready, P., 1999. Estuarine adjustment to changes in river flow and tidal mixing. J. Phys. Oceanogr. 29, 708–726. http://dx.doi.org/10.1175/1520-0485(1999)029%3C0708:EATCIR%3E2.0.CO;2.
MacCready, P., 2007. Estuarine adjustment. J. Phys. Oceanogr. 37, 2133–2145. http://dx.doi.org/10.1175/JPO3082.1.
MacCready, P., 2011. Calculating estuarine exchange flow using isohaline coordinates. J. Phys. Oceanogr. 41, 1116–1124. http://dx.doi.org/10.1175/2011JPO4517.1.
MacVean, L.J., Stacey, M.T., 2011. Estuarine dispersion from tidal trapping: a new analytical framework. Estuaries Coasts 34, 45–59. http://dx.doi.org/10.1007/s12237-010-9298-x.
MacWilliams, M.L., Bever, A.J., Gross, E.S., Ketefian, G.S., Kimmerer, W.J., 2015. Three-dimensional modeling of hydrodynamics and salinity in the San Francisco Estuary: an evaluation of model accuracy, X2, and the low salinity zone. San Franc. Estuary Watershed Sci. 13 (1). http://escholarship.org/uc/item/7x65r0tf.
Manfree, A.D., 2014. Historical Ecology. In: Moyle, P.B., Manfree, A.D., Fiedler, P.L. (Eds.), Suisun Marsh: Ecological History and Possible Futures. University of California Press, Berkeley, California, USA, pp. 9–44.
McCollum, W.S., 1850. 1960. California as I Saw It; Pencillings by the Way of its Gold and Gold Diggers, and Incidents of Travel by Land and Water. Talisman Press. Los Gatos, California, USA. Courtesy of Library of Congress.
Monismith, S.G., 2016. A note on Delta outflow. San Franc. Estuary Watershed Sci. 14 (3). http://escholarship.org/uc/item/89k7b61m.
Monismith, S.G., 2017. An integral model of unsteady salinity intrusion in estuaries. J. Hydraul. Res. http://dx.doi.org/10.1080/00221686.2016.1274682.
Monismith, S.G., Kimmerer, W.J., Burau, J.R., Stacey, M.T., 2002. Structure and flow-induced variability of the subtidal salinity field in northern San Francisco Bay. J. Phys. Oceanogr. 32, 3003–3019. http://dx.doi.org/10.1175/1520-0485(2002)032<3003:SAFIVO> 2.0.CO;2.
Mount, J., Twiss, R., 2005. Subsidence, sea level rise, and seismicity in the Sacramento-San Joaquin Delta. San Franc. Estuary Watershed Sci. 3 (1). http://escholarship.org/uc/item/4k44725p.
Moyle, P.B., Bennet, W.A., Fleenor, W.E., Lund, J.R., 2010. Habitat variability and complexity in the upper San Francisco Estuary. San Franc. Estuary Watershed Sci. 8 (3). http://escholarship.org/uc/item/0kf0d32x.
[NOAA] National Oceanic and Atmospheric Administration, 2016. Mean Sea Level Trend: 9414290 San Francisco, California. 〈http://tidesandcurrents.noaa.gov/sltrends/sltrends station.shtml?id=9414290〉. (Accessed 5 July 2016).
Payson, A.H., Government Printing Office, 1885. Annual Report of the Chief of Engineers, United States Army, to the Secretary of War. House of Representatives, 49th Congress, 1st Session, Ex. Doc. 1, pt. 2, vol. II.
Ralston, D.K., Geyer, W.R., Lerczak, J.A., 2008. Subtidal salinity and velocity in the Hudson River estuary: observations and modeling. J. Phys. Oceanogr. 38, 753–770. http://dx.doi.org/10.1175/2007JPO3808.1.
Rayson, M.D., Gross, E.S., Hetland, R.D., Fringer, O.B., 2017. Using an isohaline flux analysis to predict the salt content in an unsteady estuary. J. Phys. Oceanogr (In preparation).
[RMA] Resource Management Associates, 2005. Flooded Islands Pre-feasibility Study: RMA Delta Model calibration report. Prepared for the California Department of Water Resources for submittal to California Bay–Delta Authority. Fairfield, California, USA, pp. 1–158. 〈http://www.water.ca.gov/frankstract/docs/(8)RMA-Calibration%20Report.pdf〉. (Accessed 5 July 2016).
Rose, A.H., Manson, M., Grunsky, C.E., State Printing Office, Sacramento, California, USA, 1895. Report of the Commissioner of Public Works to the Governor of California.
Sacramento Daily Union, 1862. Is the Sacramento Valley inhabitable? March 24. Courtesy of California Digital Newspaper Collection.
[SFEI-ASC] San Francisco Estuary Institute-Aquatic Sciences Center, 2014. Natural Flow Hydrodynamic Modeling Technology Support Phase 1 Technical Memorandum. Prepared for the Metropolitan Water District of Southern California. San Francisco Estuary Institute-Aquatic Sciences Center, Richmond, California, USA (Accessed 5 July 2015). http://www.baydeltalive.com/docs/10117.
Schoellhamer, D.H., 2001. Influence of salinity, bottom topography, and tides on locations of estuarine turbidity maxima in northern San Francisco Bay. In: McAnally, W.H., Mehta, A.J. (Eds.), Coastal and Estuarine Fine Sediment Processes. Elsevier, pp. 343–356.
Simpson, J.H., Brown, J., Matthews, J., Allen, G., 1990. Tidal straining, density currents, and stirring in the control of estuarine stratification. Estuaries 13, 125–132. http://dx.doi.org/10.2307/1351581.
Stacey, M.T., Burau, J.R., Monismith, S.G., 2001. Creation of residual flows in a partially stratified estuary. J. Geophys. Res. 106 (C8), 17013–17038. http://dx.doi.org/10.1029/2000JC000576.
Stommel, H., Farmer, H.G., 1953. Control of salinity in an estuary by a transition. J. Mar. Res. 12, 12–20.
Thayer, 1859. U.S. v. Anastasio Chaboya, Land Case No. 406 ND [Sanjon de los Mequelemnes], U.S. District Court, Northern District. Courtesy of The Bancroft Library, University of California, Berkeley.
Thompson, J., 2006. Early reclamation and abandonment of the central Sacramento-San Joaquin Delta. Sacramento Hist. J. 6 (1–4), 41–72.

Thornton, S.R., 1859. U.S. v. Anastasio Chaboya, Land Case No. 406 ND, Sanjon de los Miquelemes, U.S. District Court, Northern District. 200. Courtesy of The Bancroft Library, University of California, Berkeley.

[USGS] U.S. Geological Survey, 2016. Water Quality of San Francisco Bay. ⟨http://sfbay.wr.usgs.gov/access/wqdata/index.html⟩. (Accessed 5 July 2016).

Walters, R.A., Gartner, J.W., 1985. Subtidal sea level and current variations in the northern reach of San Francisco Bay. Estuar. Coast. Shelf Sci. 21, 17–32. http://dx.doi.org/10.1016/0272-7714(85)90003-4.

Walters, R.A., Cheng, R.T., Conomos, T.J., 1985. Time scales of mixing processes of San Francisco Bay waters. Hydrobiologia 129, 13–36. http://dx.doi.org/10.1007/BF00048685.

Wang, R., Ateljevich, E., 2012. A continuous surface elevation map for modeling. In: Finch, R. (Ed.), Methodology for flow and salinity estimates in the Sacramento–San Joaquin Delta and Suisun Marsh, 33rd annual progress report to the State Water Resources Control Board. California Department of Water Resources, Sacramento, California, USA, pp. 121–146. (Accessed 5 July 2016). http://baydeltaoffice.water.ca.gov/modeling/deltamodeling/AR2012/Method DeltaModel 2012 FullReport FINAL Web.pdf.

Wang, Z.B., Van Maren, D.S., Ding, P.X., Yang, S.L., Van Prooijen, B.C., De Vet, P.L.M., Winterwerp, J.C., De Vriend, H.J., Stive, M.J.F., He, Q., 2015. Human impacts on morphodynamic thresholds in estuarine systems. Cont. Shelf Res. 111 (B), 174–183. http://dx.doi.org/10.1016/j.csr.2015.08.009.

Warner, J.C., Sherwood, C.S., Arango, H.G., Signell, R.P., 2005. Performance of four turbulence closure models implemented using a generic length scale method. Ocean Model. 8, 81–113. http://dx.doi.org/10.1016/j.ocemod.2003.12.003.

Whipple, A.A., Grossinger, R.M., Rankin, D., Stanford, B., Askevold, R.A., 2012. Sacramento–San Joaquin Delta Historical Ecology Investigation: Exploring Pattern and Process. San Francisco Estuary Institute, Richmond, California, USA (Accessed 5 July 2016). http://www.sfei.org/DeltaHEStudy.

Willmott, C.J., 1981. On the validation of models. Phys. Geogr. 2, 184–198. http://dx.doi.org/10.1080/02723646.1981.10642213.